Advanced Calibration for Device Simulation User Guide

Version N-2017.09, September 2017

SYNOPSYS®

Copyright and Proprietary Information Notice

Destination Control Statement

All technical data contained in this publication is subject to the export control laws of the United States of America. Disclosure to nationals of other countries contrary to United States law is prohibited. It is the reader's responsibility to determine the applicable regulations and to comply with them.

Disclaimer

SYNOPSYS, INC., AND ITS LICENSORS MAKE NO WARRANTY OF ANY KIND, EXPRESS OR IMPLIED, WITH REGARD TO THIS MATERIAL, INCLUDING, BUT NOT LIMITED TO, THE IMPLIED WARRANTIES OF MERCHANTABILITY AND FITNESS FOR A PARTICULAR PURPOSE.

Trademarks

Synopsys and certain Synopsys product names are trademarks of Synopsys, as set forth at https://www.synopsys.com/company/legal/trademarks-brands.html.
All other product or company names may be trademarks of their respective owners.

Third-Party Links

Any links to third-party websites included in this document are for your convenience only. Synopsys does not endorse and is not responsible for such websites and their practices, including privacy practices, availability, and content.

Synopsys, Inc.
690 E. Middlefield Road
Mountain View, CA 94043
www.synopsys.com

Contents

Contents

About This Guide

The Synopsys Sentaurus™ Device tool is a quantum drift-diffusion device simulator for solving the semiconductor equations in one, two, or three spatial dimensions.

Extensions for hydrodynamic transport, solution of the heat conduction equation, and many other features are available as well. Because of the large number of models and the corresponding model parameters and their dependency on fabrication processes and device types, it is difficult to derive automatically a well-adjusted device simulation environment for specific simulation tasks. Therefore, preselection of models and precalibration of parameter sets are necessary. This preselection and precalibration is called Advanced Calibration Device.

This user guide describes the contents, the use, and the syntax of the Advanced Calibration files for Sentaurus Device. It is intended for users who are familiar with the use of Sentaurus Device and want to obtain a higher accuracy in device simulation. For detailed information about Sentaurus Device, refer to the *Sentaurus™ Device User Guide*.

Synopsys is working continually on improving the simulation models and optimizing the model parameters for the latest technology nodes. This effort is based on long-standing experience of model calibration for customers and a comprehensive, growing knowledge about device simulation methodologies. The variety of partners and data ensures that systematic and random errors in experimental work are minimized in this model representation.

Advanced Calibration Device provides users with a set of parameters for CMOS technologies from micrometer dimensions down to the 14 nm node, including planar gate-first and gate-last technologies, nonplanar technologies for the 14 nm node, and technologies beyond 14 nm likely based on novel channel materials (SiGe, Ge, and III–V). In addition, Advanced Calibration Device delivers parameter sets for bipolar CMOS DMOS (BCD) technologies, silicon and SiC power devices, GaN HEMTs, and InGaAs devices.

The requirements of device simulation and device calibration approaches are discussed.

This user guide is designed to give fast access to parameter sets and model selections needed for simulation. Therefore, the first chapters provide a guide from the simulation problem to the selection of parameter sets and device models.

Related Publications

For additional information, see:

- The TCAD Sentaurus release notes, available on the Synopsys SolvNet® support site (see Accessing SolvNet).
- Documentation available on SolvNet at https://solvnet.synopsys.com/DocsOnWeb.

Conventions

The following conventions are used in Synopsys documentation.

Convention	Description
Blue text	Identifies a cross-reference (only on the screen).
Bold text	Identifies a selectable icon, button, menu, or tab. It also indicates the name of a field or an option.
`Courier font`	Identifies text that is displayed on the screen or that the user must type. It identifies the names of files, directories, paths, parameters, keywords, and variables.
Italicized text	Used for emphasis, the titles of books and journals, and non-English words. It also identifies components of an equation or a formula, a placeholder, or an identifier.
Key+Key	Indicates keyboard actions, for example, Ctrl+I (press the I key while pressing the Control key).
Menu > Command	Indicates a menu command, for example, **File > New** (from the **File** menu, select **New**).

Customer Support

Customer support is available through the Synopsys SolvNet customer support website and by contacting the Synopsys support center.

Accessing SolvNet

The SolvNet support site includes an electronic knowledge base of technical articles and answers to frequently asked questions about Synopsys tools. The site also gives you access to a wide range of Synopsys online services, which include downloading software, viewing documentation, and entering a call to the Support Center.

To access the SolvNet site:

1. Go to the web page at https://solvnet.synopsys.com.
2. If prompted, enter your user name and password. (If you do not have a Synopsys user name and password, follow the instructions to register.)

If you need help using the site, click **Help** on the menu bar.

Contacting Synopsys Support

If you have problems, questions, or suggestions, you can contact Synopsys support in the following ways:

- Go to the Synopsys Global Support Centers site on synopsys.com. There you can find e-mail addresses and telephone numbers for Synopsys support centers throughout the world.
- Go to either the Synopsys SolvNet site or the Synopsys Global Support Centers site and open a case online (Synopsys user name and password required).

Contacting Your Local TCAD Support Team Directly

Send an e-mail message to:

- support-tcad-us@synopsys.com from within North America and South America.
- support-tcad-eu@synopsys.com from within Europe.
- support-tcad-ap@synopsys.com from within Asia Pacific (China, Taiwan, Singapore, Malaysia, India, Australia).
- support-tcad-kr@synopsys.com from Korea.
- support-tcad-jp@synopsys.com from Japan.

CHAPTER 1 Using Advanced Calibration File of Sentaurus Device

This chapter gives a brief introduction to the use of Advanced Calibration in a device simulation with Sentaurus Device.

Overview

Advanced Calibration Device is a selection of models and parameters that is recommended to be used for device simulation of certain device types and technologies. This selection of models and parameters is contained in text files, which can be opened with any standard text editor.

By starting Sentaurus Device with the corresponding Advanced Calibration Device command file section and loading the Advanced Calibration Device parameter file from that command file, the standard calibration of Synopsys is selected.

For more information about how to use the command file, which defines the models, and the parameter file, which defines the parameters of the models selected in the command file, refer to the *Sentaurus™ Device User Guide*.

Location of Advanced Calibration File

For each release of Synopsys TCAD, there are new Advanced Calibration Device files that include the latest set of models and parameters. The parameter files are stored in the `MaterialDB` folder of the standard installation of Sentaurus Device.

Currently, the available material-related files are `Silicon.par`, `Germanium.par`, `SiliconGermanium.par`, `Siliconc100.par`, `SiliconGermaniumc100.par`, `Siliconc110.par`, `SiliconGermaniumc110.par`, `SiliconCarbide.par`, `AlGaN.par`, `AlInGaN.par`, `AlInN.par`, `AlN.par`, `GaAs.par`, `GaN.par`, `InAs.par`, `InGaAs.par`, `InGaN.par`, `InN.par`, `4H-SiC.par`, and `6H-SiC.par`.

The parameter file and command file sections for the Advanced Calibration of Sentaurus Device are described in this user guide. They represent Version N-2017.09 of Advanced Calibration Device.

Using Advanced Calibration Device

To use the Advanced Calibration of Sentaurus Device, you can look up the parameter files and the command files that are best suited for your device and technology requirements in Chapter 3 on page 5.

As a result of the European Union (EU) projects DEEPEN and III-V-MOS, additional parameter sets have been generated that complement the general parameter files of Advanced Calibration of Sentaurus Device. These parameter files will be fully integrated in later releases.

For Version N-2017.09, the related parameter files can be delivered on request. See Contacting Your Local TCAD Support Team Directly on page ix.

In addition, the following TCAD simulation projects are available and can be delivered on request:

- III-V-arsenide channel DG-FET
- III-V-arsenide channel FDSOI-FET
- III-V-arsenide channel FinFET

Each project contains documentation that explains the project, the parameter settings, and the models in detail.

CHAPTER 2 Content of Advanced Calibration Device

This chapter specifies the target devices and technologies for Advanced Calibration Device.

Target Devices and Technologies

This version of Advanced Calibration Device focuses on deep-submicron technology nodes down to 7 nm, based on silicon, germanium, SiGe, or III–V channel materials. In addition, parameters and models for silicon smart-power and power devices (IGBT, LDMOS, NMOS, PMOS), GaN HEMTs, InGaAs channel devices, SiC diodes, and SiC FETs are provided and discussed.

The main process features of planar and nonplanar bulk and SOI technology nodes that should be covered by the model and parameter sets are:

- Stress and crystallographic orientation engineering
- Poly/SiON, or SiO_2, or metal/HfO_2/SiON, or SiO_2 gate stacks
- Gate-first and gate-last technologies
- Silicon, germanium, SiGe, and InGaAs channel

The main device types included are:

- Low-power and high-performance NMOS and PMOS with silicon, germanium, SiGe, and InGaAs channel
- Selected silicon smart-power and power devices
- GaN HEMTs
- SiC diodes and FETs

For the abovementioned devices and technologies, Advanced Calibration Device provides model selections and parameter sets for the simulation of the following device properties:

- Electrostatic properties and quantization
- Low-field and high-field mobility
- Stress dependency of mobility

NOTE The parameter sets must be considered as inital parameter sets, that is, starting points for further calibration.

CHAPTER 3 Guide to Device Simulation

This chapter provides a guide for the selection of parameter sets and device models.

In this chapter, users can select parameter sets and models quickly. The chapter is organized in the following way: Table 1 and Table 2 present typical simulation cases. In the tables, a path is defined that can be used to select the proper device simulation parameter set and the appropriate `Physics` section for the command file.

Specifying Simulation Cases

In Table 1 and Table 2, the characters A to I indicate different paths that are described in detail in the following sections.

Table 1 Specifying the simulation case: CMOS

Node	**> 130 nm**	**32–130 nm**			**14–32 nm**				**< 14 nm**								
Selection path	A	B	C	C	B	C	C	C	E	D	E	E	I	I	E	E	E
Planar bulk and SOI	X	X	X	X	X	X	X	X									
FinFET									X		X	X	X				
Nanowire														X	X	X	X
Thin-layer SOI										X							
Si	X	X	X		X	X		X	X	X					X		
SiGe				X			X				X					X	
Ge												X					X
InGaAs													X	X			
Gate-first	X	X			X												
Gate-first with metal gate			X	X		X	X										
Gate-last with metal gate								X	X	X	X	X	X	X	X	X	X
Without stress	X														X		
With stress		X	X	X	X	X	X	X	X	X	X	X	X	X		X	X

Table 2 Specifying the simulation case: Smart power and power

Node	HVMOS	LDMOS	HEMT	Diode	IGBT
Selection path	F	F	G	H	F
Si	X	X			X
SiC				X	
GaN			X		

Access to Parameter Files and Model Frameworks

The following sections give access to the model frameworks and the parameter files.

Path A: Basic CMOS Simulation Command File Sections

For quantization, the density gradient model of Sentaurus Device is used (`eQuantumPotential` and `hQuantumPotential`). However, for technologies with gate oxide thicknesses greater than 3 nm, quantum correction can be neglected without affecting the simulation of the gate capacitance and the threshold voltage too much.

The orientation of the conducting interface is detected automatically. However, the channel or the current flow direction must be defined manually using the correct mobility parameter file. The corresponding parameter files are located in `$STROOT/tcad/$STRELEASE/lib/sdevice/MaterialDB`. For more information about the handling and loading of parameter files, refer to the *Sentaurus™ Device User Guide*.

For the <110> channel direction, `Siliconc110.par` must be loaded. For the <100> channel direction, `Siliconc100.par` must be loaded.

```
Physics {Fermi}

Physics (Material="Silicon") {
   eQuantumPotential(AutoOrientation density)
   hQuantumPotential(AutoOrientation density)
   Mobility (Enormal (IALMob(AutoOrientation)) HighFieldSaturation)
   # For PMOS, it is useful to use PhononCombination=2 in the IALMob
   EffectiveIntrinsicDensity(OldSlotboom)
   Recombination(SRH)
   # Recombination(SRH Band2Band)  # For off-current calculation, band-to-band
                                   # tunneling models must be switched on.
}
```

Path B: Adding Influence of Mechanical Stress to Physics Section Shown Under Path A

Taking into account mechanical stress, the low-field mobility model must be combined with a model describing the stress influence. There are two ways to model the mobility change by mechanical stress:

- First, you can use the `eSubband` and `hSubband` models for a physically based calculation of the mobility enhancement by mechanical stress in silicon devices that is directly based on band structure and subbands. For the subband models, the channel direction must be set in the command file when it is not the <110> channel.
- Second, you can use the `MCmob` PMI model (parameters are extracted from Sentaurus Device Monte Carlo) or the `SBmob` PMI model (parameters are extracted from Sentaurus Band Structure). For `MCmob` and `SBmob`, the channel direction must be set in the parameter file (see Appendix A on page 85).

The orientation of the conducting interface is detected automatically. However, the channel or the current flow direction must be defined manually using the correct mobility parameter file. The corresponding parameter files are located in `$STROOT/tcad/$STRELEASE/lib/sdevice/MaterialDB`. For more information about the handling and loading of parameter files, refer to the *Sentaurus™ Device User Guide*.

For the <110> channel direction, `Siliconc110.par` must be loaded. For the <100> channel direction, `Siliconc100.par` must be loaded.

With subband models, the following syntax must be used:

```
Physics {Fermi}

Physics (Material="Silicon") {
   eQuantumPotential(AutoOrientation density)
   hQuantumPotential(AutoOrientation density)
   Mobility (Enormal (IALMob(AutoOrientation)) HighFieldSaturation)
   # For PMOS, it is useful to use PhononCombination=2 in the IALMob
   EffectiveIntrinsicDensity(OldSlotboom)
   Recombination(SRH)
   # Recombination(SRH Band2Band)  # For off-current calculation, band-to-band
                                   # tunneling models must be switched on.
```

```
   eMultivalley(MLDA kpDOS -density)   # hMultivalley for holes
   Piezo (
      Model (
         Mobility (
            saturationfactor=0.2
            eSubband(Fermi EffectiveMass Scattering(MLDA))
               # eSubband(Fermi EffectiveMass Scattering(MLDA) -RelChDir110)
               # for <100> channel
               # hSubband(Fermi EffectiveMass Scattering(MLDA)) for holes
               # for holes, the replacement of the option Fermi by the option
               # Doping can result in speedup of the simulation
         )
         DOS(eMass hMass)
         DeformationPotential(Minimum ekp hkp)
      )
   )
}
```

With `MCmob` or `SBmob`, the following syntax must be used:

```
Physics {Fermi}

Physics (Material="Silicon") {
   eQuantumPotential(AutoOrientation density)
   hQuantumPotential(AutoOrientation density)
   Mobility (Enormal (IALMob(AutoOrientation)) HighFieldSaturation)
   # For PMOS, it is useful to use PhononCombination=2 in the IALMob
   EffectiveIntrinsicDensity(OldSlotboom)
   Recombination(SRH)
   # Recombination(SRH Band2Band)  # For off-current calculation, band-to-band
                                   # tunneling models must be switched on.

   Piezo (
      Model (
         Mobility (
            saturationfactor=0.2
            efactor(Kanda sfactor=SBmob(Type=0))    # Type=1 for holes
            #efactor(Kanda sfactor=MCmob(Type=0))   # when using MCmob
         )
         DOS(eMass hMass)
         DeformationPotential(Minimum ekp hkp)
      )
   )
}
```

The command file section above is designed for electron transport (NMOS). For hole transport (PMOS), you must replace `eSubband` with `hSubband`, `eMultivalley` with `hMultivalley`, and specify `Type=1` for `MCmob` and `SBmob`.

Path C: Adding High-k Mobility Degradation to Physics Section Shown Under Path B

The orientation of the conducting interface is detected automatically. However, the channel or the current flow direction must be defined manually using the correct mobility parameter file. The corresponding parameter files are located in `$STROOT/tcad/$STRELEASE/lib/sdevice/MaterialDB`. For more information about the handling and loading of parameter files, refer to the *Sentaurus™ Device User Guide*.

For the silicon <110> channel direction, `Siliconc110.par` must be loaded. For the silicon <100> channel direction, `Siliconc100.par` must be loaded. For the SiGe <110> channel direction, `SiliconGermaniumc110.par` must be loaded. For the SiGe <100> channel direction, `SiliconGermaniumc100.par` must be loaded.

```
Physics {Fermi}

Physics (Material="Silicon") {
#or Physics (Material="SiliconGermanium") {
   eQuantumPotential(AutoOrientation density)
   hQuantumPotential(AutoOrientation density)
   Mobility (
      Enormal (
         IALMob(AutoOrientation)
         # For PMOS, it is useful to use PhononCombination=2 in the IALMob
         RPS                          # Used for remote phonon scattering (RPS)
         NegInterfaceCharge (SurfaceName="s1")
                                      # Used for remote Coulomb scattering (RCS)
                                      # and remote dipole scattering (RDS)
         PosInterfaceCharge (SurfaceName="s1")
                                      # Used for RCS and RDS
      )
      HighFieldSaturation)
   EffectiveIntrinsicDensity(OldSlotboom)
                           # For SiGe with high Ge mole fraction or for pure
                           # Ge, it is recommended to switch off the Fermi
                           # correction and to use
                           # EffectiveIntrinsicDensity(OldSlotboom NoFermi)
   Recombination(SRH)
   # Recombination(SRH Band2Band)  # For off-current calculation, band-to-band
                                   # tunneling models must be switched on.
```

```
    eMultivalley(MLDA kpDOS -density)   # hMultivalley for holes
                    # For SiGe, use eMultivalley(MLDA kpDOS parfile -density)
    Piezo (
       Model (
          Mobility (
             saturationfactor=0.2
             eSubband(Fermi EffectiveMass Scattering(MLDA))
                # eSubband(Fermi EffectiveMass Scattering(MLDA) -RelChDir110)
                # for <100> channel
                # hSubband(Fermi EffectiveMass Scattering(MLDA)) for holes
                # for holes, the replacement of the option Fermi by the option
                # Doping can result in speedup of the simulation
          )
          DOS(eMass hMass)
          DeformationPotential(Minimum ekp hkp)
       )
    )
}
```

The surface name specifies the surface or interface that causes the mobility degradation, for example, the HfO_2–oxide interface in the high-k gate stack of a MOS transistor. The surface must be defined in the `Math` section of the command file. For more detailed explanations of the high-k mobility degradation models, see Chapter 5 on page 27.

Path D: Thin-Layer MOS Simulations – Including Thin-Film Effects

The `Mobility` command in the `Physics` section of Path C must be replaced by:

```
Mobility (
   ThinLayer (IALMob(AutoOrientation))
   # For PMOS, it is useful to use PhononCombination=2 in the IALMob
      Enormal (
         RPS                          # Used for remote phonon scattering (RPS)
         NegInterfaceCharge (SurfaceName="s1")
                                      # Used for remote Coulomb scattering (RCS)
                                      # and remote dipole scattering (RDS)
         PosInterfaceCharge (SurfaceName="s1")
                                      # Used for RCS and RDS
      )
      HighFieldSaturation)
```

All other options and statements remain the same.

Path E: FinFET Simulations

The same `Physics` section as in Path C can be used. The `AutoOrientation` flag for the density gradient model must be switched on. As a starting point for calibration, the same parameter files `Siliconc110.par`, `Siliconc100.par`, `SiliconGermaniumc110.par`, and `SiliconGermaniumc100.par` can be used as well. However, because the interface quality of the fin sidewalls can be very different from the interface quality of a planar transistor, parameter adjustments are often necessary.

In general, it is observed that the FinFET electron inversion mobility is higher at the (110) sidewalls than in planar (110) transistors [1].

Table 3 and Table 4 show the current approach for modeling planar and nonplanar FinFET devices regarding orientation-related parameters.

Table 3 Parameter sets for planar FETs and FinFETs with silicon channel

Device	Number of conducting planes	Conducting plane orientation	Channel orientation	Parameter set
Planar MOS	1	(100)	<100>	`Siliconc100.par`
Planar MOS	1	(110)	<100>	`Siliconc100.par`
Planar MOS	1	(100)	<110>	`Siliconc110.par`
Planar MOS	1	(110)	<110>	`Siliconc110.par`
FinFET	3	(100)	<100>	`Siliconc100.par`
FinFET	3	(100) (110)	<110> <110>	`Siliconc110.par`

Table 4 Parameter sets for planar FETs and FinFETs with SiGe channel

Device	Number of conducting planes	Conducting plane orientation	Channel orientation	Parameter set
Planar MOS	1	(100)	<100>	`SiliconGermaniumc100.par`
Planar MOS	1	(110)	<100>	`SiliconGermaniumc100.par`
Planar MOS	1	(100)	<110>	`SiliconGermaniumc110.par`
Planar MOS	1	(110)	<110>	`SiliconGermaniumc110.par`
FinFET	3	(100)	<100>	`SiliconGermaniumc100.par`
FinFET	3	(100) (110)	<110> <110>	`SiliconGermaniumc110.par`

For very short gate lengths, less than 15 nm, the isotropic density gradient model can overestimate the leakage current in the transport direction (source-drain tunneling). In those cases, the `alpha` parameter in the density gradient model can help to suppress the current in the transport direction. For FinFET simulations with a gate length below 15 nm, using `alpha(1)` < 0.1 can be a good starting point. For more information about the handling and use of the anisotropic density gradient model, refer to the *Sentaurus™ Device User Guide*.

NOTE Using the `DOS(eMass hMass)` model in the `Piezo` section and the temperature equation at the same time can result in convergence problems. The use of the `NumericalIntegration` flag in `DOS(hMass(NumericalIntegration))` can improve the numeric behavior.

Path F: Smart-Power HVMOS and LDMOS Devices

In principle, Path A should be used for silicon-based smart-power devices exhibiting a traditional polysilicon/oxide gate stack when no mechanical stress occurs in the structure. When mechanical stress occurs in the structure, Path B must be used. However, in many cases, the linear piezo model may be sufficient because the mechanical stress is mostly smaller than in deep-submicron devices. For complex devices or 3D simulation structures, it may be necessary to simplify the model complexity to reduce simulation time or to achieve convergence. The following simplified `Physics` section can be applied in those cases:

```
Physics {Fermi}

Physics (Material="Silicon") {
   Mobility (Enormal (IALMob(AutoOrientation)) HighFieldSaturation)
   # For PMOS, it is useful to use PhononCombination=2 in the IALMob
   EffectiveIntrinsicDensity(OldSlotboom)
   Recombination (Auger SRH(DopingDep TemDep))
   # Recombination(Auger SRH(DopingDep TemDep) Band2Band)
      # For off-current calculation, band-to-band tunneling models must be
      # switched on.
}
```

Quantum correction is neglected here, resulting in better simulation performance. The loss of accuracy can mostly be compensated by a corresponding workfunction shift and a reduction of the gate isolation permittivity. For devices with a gate isolation oxide thickness greater than 3 nm, the influence of the quantum correction decreases. The `Physics` section above is designed for I_d–V_d and I_d–V_g simulations, but it does not include the models for breakdown, substrate current, and complex electrostatic discharge (ESD) simulation. In addition, the commands necessary for consideration of self-heating must be switched on.

Parameter files and the model section have been tested for LDMOS devices. No tests and investigations have been conducted for IGBTs, thyristors, or bipolar devices.

Path G: GaN HEMT Simulations

For numeric reasons, the well-known extended Canali model is used to simulate high-field effects. The use of the transferred electron models, which are physically more suited to the simulation of GaN HEMTs, is limited because of poor convergence.

It is known that the surface roughness at interfaces to the GaN channel influences the channel mobility. However, because of missing model parameters and the need for further investigation of the mobility in the 2D electron gas, the model is not included here. Typically, it is advisable to use the density gradient model for quantum correction. For numeric reasons and because of missing parameters, this model is not included here.

The values for the trap concentration and the energy level given here are typical for nitride-passivated GaN HEMTs. However, the actual values depend on the device and can be different from the values presented here. In addition to the interface traps shown in the input file section here, bulk traps are important and must be implemented into the simulation, for example, when investigating current collapse effects.

The parameter files `GaN.par`, `AlGaN.par`, `AlN.par`, `InGaN.par`, and `InN.par`, which contain the material parameters for the III–V nitride wide-bandgap materials, are located in `$STROOT/tcad/$STRELEASE/lib/sdevice/MaterialDB`. For more information about the handling and loading of parameter files, refer to the *Sentaurus™ Device User Guide*.

The `Physics` section that should be used together with the parameter files is:

```
Physics {
   Mobility (
      DopingDependence(Arora)  # Masetti model can be used as well. Model
                               # parameters are in the parameter files
                               # (GaN.par, AlGaN.par, and AlN.par).
      HighFieldSaturation
   )
   EffectiveIntrinsicDensity(noBandGapNarrowing)
   Piezoelectric_Polarization(strain)
   Recombination(Radiative)
   Fermi
   Thermodynamic
   Thermionic
   HeteroInterface
   eBarrierTunneling "STUN"
   eBarrierTunneling "DTUN"
}

Physics (MaterialInterface="AlGaN/Nitride") {
   Traps(Donor Level Conc=1E13 EnergyMid=0.4 FromMidBandGap)
                     # The values for the trap concentration and the energy
```

```
                    # are calibration parameters.
   Piezoelectric_Polarization(strain activation=0)
}
```

Path H: SiC Diode Simulations

The parameter files `4H-SiC.par` and `6H-SiC.par`, which contain the material parameters for the SiC-based wide-bandgap materials, are located in `$STROOT/tcad/$STRELEASE/lib/sdevice/MaterialDB`. For more information about the handling and loading of parameter files, refer to the *Sentaurus™ Device User Guide*.

The `Physics` section that should be used together with the parameter files is:

```
Physics {
   eMobility (
      DopingDependence(Arora)     # For 6H-SiC, Arora parameters are not
                                  # available in the parameter file.
                                  # Therefore, it is recommended to switch
                                  # to the Masetti model.
      HighFieldSaturation
   )
   hMobility (
      DopingDependence(Arora)     # For 6H-SiC, Arora parameters are not
                                  # available in the parameter file.
                                  # Therefore, it is recommended to switch to
                                  # the Masetti model.
      HighFieldSaturation
   )
   EffectiveIntrinsicDensity(Slotboom noFermi)
   IncompleteIonization
   Recombination(SRH(DopingDep TempDep Tunneling) Band2Band Avalanche (Okuto))
                                  # For forward characteristics, the commands
                                  # Band2Band and Tunneling can be neglected.
                                  # This can improve the convergence behavior.
   Fermi
   #Thermodynamic                 # Add for thermodynamic simulations
   #AnalyticTEP                   # Add for thermodynamic simulations
   Temperature=300.0
   eBarrierTunneling "NLM" (Twoband Transmission)
                        # nonlocal mesh definition in Math section necessary
   Traps (
      Donor Level EnergyMid=1.0 FromConductionband Conc=1e14
      eXSection=1.0e-12 hXSection=1.0e-12 PooleFrenkel TrapVolume=1.0e-9
      HuangRhys=0.1 PhononEnergy=0.05 eBarrierTunneling (Twoband)
```

```
   )                    # Bulk traps are often necessary for the physically
                        # correct calculation of the thermal behavior of the
                        # reverse leakage current.
}

Physics (Electrode="top") {
   #MSPeltierHeat                # Add for thermodynamic simulations
   Schottky BarrierLowering
}
```

Depending on how the mobility model has been calibrated, that is, if the total chemical concentration or the active concentration has been used, the `IncompleteIonization` statement can be added to the `Mobility` section. For holes, the suggested parameters for the Arora model in `4H-SiC.par` were calibrated to the total acceptor concentration. In addition, scattering on the neutral impurities is often comparable to scattering on the ionized impurities for 4H-SiC p-type layers.

NOTE Using the `IncompleteIonization` model can cause convergence problems.

To distinguish between both cubic and hexagonal 4H-SiC lattice sites, the following option can be activated in the `IncompleteIonization` subsection of the `Physics` section of the command file:

```
IncompleteIonization(Split (Doping="NitrogenActive" Weights=(0.5 0.5)))
```

The corresponding parameters must be defined in the parameter file. Precalibrated values are in the `4H-SiC.par` and `6H-SiC.par` files for phosphorus and nitrogen. For phosphorus, the parameters corresponding to hexagonal sites are active, and modification of the `datexcodes.txt` file is necessary to treat both sites.

The values for the trap concentration, the energy levels, and other parameters in the trap command are typical. However, the actual values depend on the device and can be different from the values presented here. Especially for the leakage current in reverse mode, tunneling by defect traps can play an important role and should be investigated.

The use of the `NoFermi` statement depends on the extraction of the bandgap narrowing model parameters. `NoFermi` is applied if you use parameters for bandgap narrowing that have been extracted assuming Fermi statistics.

When including heat generation and conduction, a lumped model (thermal network) using the thermal resistance of layers and material regions that are not included in the simulation can improve the simulation results.

An alternative option that is physically more suited – the `JainRoulston` model – can be used for bandgap narrowing. This option requires further testing and evaluation. For 2D and 3D

structures, anisotropic material properties for mobility, permittivity, thermal conductivity, and impact ionization must be taken into account in the simulation. This can be performed by the Sentaurus Device commands in the `Physics` section:

```
Aniso (Mobility Poisson Temperature Avalanche)
```

The corresponding parameters must be defined in the parameter file. Precalibrated values are in the `4H-SiC.par` (same as `SiliconCarbide.par`) and `6H-SiC.par` files for permittivity, thermal conductivity, impact ionization, mobility, incomplete ionization, high-field saturation, and other models.

Path I: InGaAs FinFET Simulations

For InGaAs FinFET devices with a gate width of less than 10 nm, two quantization models of Sentaurus Device are available to model quantized distributions of carriers:

- The MLDA model can be used with the `ThinLayer` flag specified in the command file to activate the size quantization with the multivalley model. For a 2D structure, the layer thickness can be extracted automatically, and the depletion at corner regions corresponds better to the results of Schrödinger equation using the `MaxFit` option. Using `MaxFitWeight=0.35` is advisable to start with, although an adjustment might be required depending on fin geometries.
- The density gradient model also can be used in combination with the multivalley model. The quantization parameter in the density gradient model (γ-parameter) depends on the layer thickness and the fin geometry. Therefore, it is advisable to perform the calibration to the solutions from the Schrödinger equation in test structures with similar channel geometry.

In addition, the inversion and accumulation layer mobility (`IALMob`) model is available to model inversion-type n-channel InGaAs FinFETs. The parameters have been calibrated to available experimental data under the condition of `PhononCombination=1`.

The parameter files `GaAs.par`, `InGaAs.par`, and `InAs.par`, which contain the material parameters for the III–V–arsenide materials, are located in `$STROOT/tcad/$STRELEASE/lib/sdevice/MaterialDB`. For more information about the handling and loading of parameter files, refer to the *Sentaurus™ Device User Guide*.

The `Physics` section that must be used together with the parameter files is:

With the MLDA model:

```
Physics {Fermi}

Physics (Material="InGaAs") {
   Mobility (
      eHighFieldSaturation     # In case of convergence problems, you can use
                               # eHighFieldSaturation(EparallelToInterface)
      Enormal(IALMob(PhononCombination=1))
   )
   EffectiveIntrinsicDensity(BandGapNarrowing(JainRoulston) NoFermi)
   Recombination(SRH Auger)
   eMultiValley(MLDA Nonparabolicity ThinLayer)
   LayerThickness(MaxFitWeight=0.35)
}
```

With the density gradient model:

```
Physics {Fermi}

Physics (Material="InGaAs") {
   Mobility (
      eHighFieldSaturation     # In case of convergence problems, you can use
                               # eHighFieldSaturation(EparallelToInterface)
      Enormal(IALMob(PhononCombination=1))
   )
   EffectiveIntrinsicDensity(BandGapNarrowing(JainRoulston) NoFermi)
   Recombination(SRH Auger)
   eMultiValley(Nonparabolicity)
   eQuantumPotential(Density)  # γ-parameter requires calibration
}
```

References

[1] C. D. Young *et al*., “(110) and (100) Sidewall-oriented FinFETs: A performance and reliability investigation,” *Solid-State Electronics*, vol. 78, pp. 2–10, December 2012.

CHAPTER 4 Guide for Calibration of Device Simulations

This chapter provides an introduction to device calibration.

The basic calibration methodology used to improve the accuracy of the simulation of CMOS devices is explained here.

Calibration Methodology

This section introduces basis aspects of the CMOS calibration methodology.

Calibration of CMOS Devices

Figure 1 shows a general flow of the calibration methodology used for CMOS devices. The different measurements and layout configurations allow you to separate device simulation model parameters. However, in many cases, iterations are necessary. In the next sections, this calibration methodology is explained in detail. For that, it is assumed that all process calibration issues are solved beforehand and the doping profile is correct.

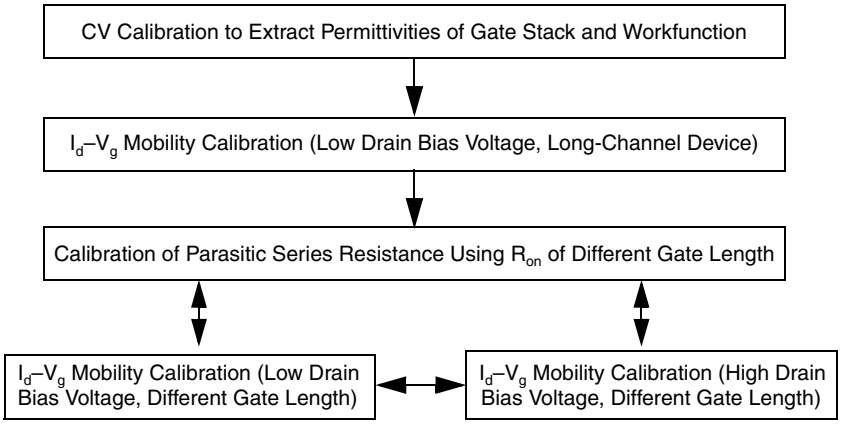

Figure 1 Calibration methodology

CV Calibration

CV calibration is the first step in the device calibration hierarchy. CV calibration is strongly connected to the doping profile and to process simulation or calibration. Because it is assumed that the doping profile is correct, the bottom of the C–V curve (region D in Figure 2) fits the experiment already. CV calibration is performed on large-area MOS transistors or MOS capacitor test structures at low frequency. Because of this, it is possible, in some cases, to have slightly different workfunctions compared to smaller transistor devices. Table 5 lists the main steps and the extracted parameters of a CV calibration.

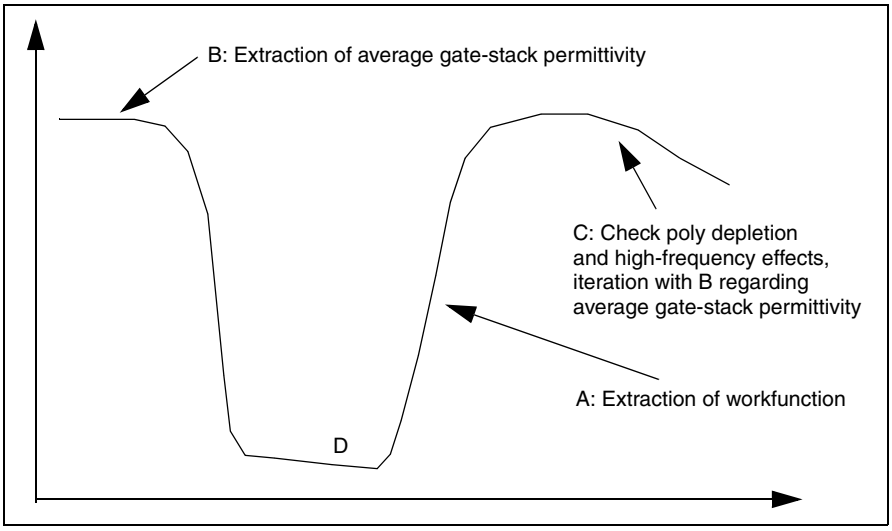

Figure 2 CV calibration methodology (NMOS)

Table 5 Main steps of CV calibration

Step	Target	Parameter to extract	Validity range of parameter	Comments
A	Region of weak or moderate inversion	Workfunction	Metal gate workfunction: NMOS (4.0–4.7 eV) PMOS (4.5–5.2 eV) Polygate barrier: –0.2 V – 0.2 V	Workfunction or barrier voltages extracted from CV and used for long-channel I–V simulation can require corrections, particularly in cases where special CV test structures are used.
B	Accumulation part of CV	Average permittivity of gate isolation	Permittivity of high-k material: 14–25 Permittivity of interfacial oxide: 3.9–6	In the case of high-k gate stacks with several material layers, first the permittivity of the interfacial oxide layer is adjusted. Then, the permittivity of the high-k material is calibrated.
C	Inversion part of CV	Poly doping in case of polygate	Depends on process conditions	

Long-Channel Id–Vg Calibration

The calibration of long-channel devices is necessary to extract low-field mobility parameters. Typically, I_d–V_g characteristics of devices with a gate length greater than 500 nm, at low drain bias voltage smaller than 100 mV, are used for this. The parameters of the mobility model are extracted in different voltage regions using an iterative process (see Figure 3, Figure 4, and Table 6 on page 22).

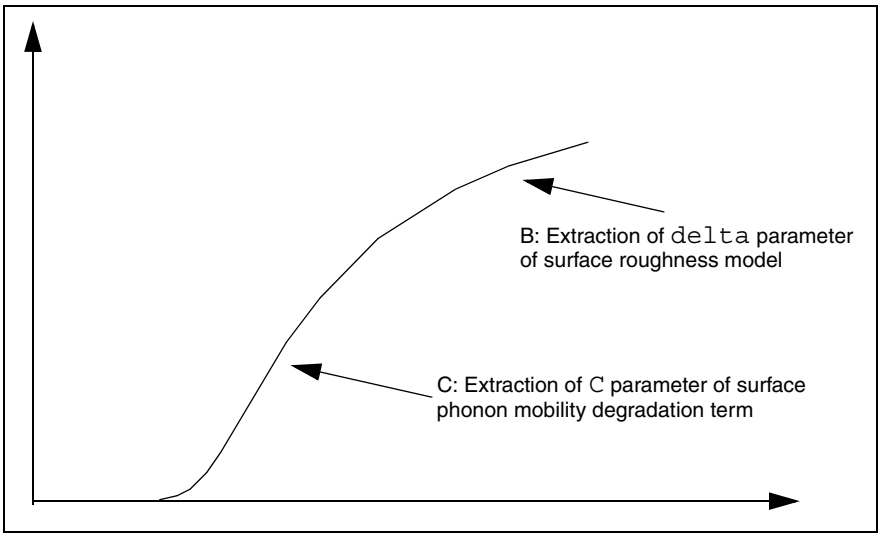

Figure 3 Long-channel I_d–V_g calibration methodology (linear scale)

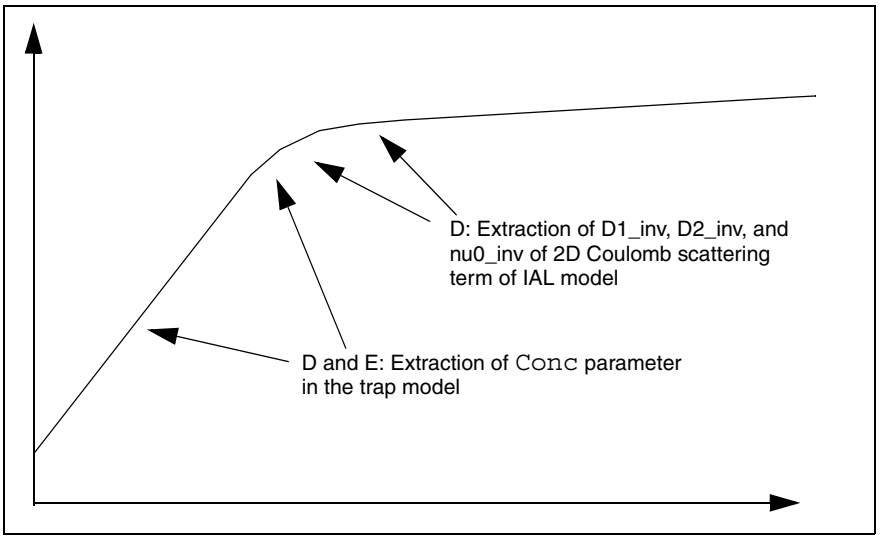

Figure 4 Long-channel I_d–V_g calibration methodology (logarithmic scale)

Table 6 Main steps of long-channel I_d–V_g calibration

Step	Target	Parameter to extract	Validity range of parameter	Comments
A	Threshold voltage	Workfunction	Depends on gate material. Stress in the metal gate as well as grain sizes and orientations influence the workfunction and can result in a dependency on gate length and geometric parameters.	Typically, metal gate workfunctions of 4.1 eV for NMOS and 4.9 eV for PMOS are used. Take initial value from CV calibration. Note there can be an influence of remote Coulomb or dipole scattering (RCS or RDS), or 2D impurity Coulomb scattering on the threshold voltage, which couples workfunction and mobility extraction.
B	Strong inversion – high gate bias voltage	`Delta` parameter of surface roughness model	Depends on process conditions and other parameters – no validity range known	Surface roughness can change when changing process conditions and surface orientations. Fine-tuning is always necessary to fit I_d–V_g characteristics.
C	Linear region of I_d–V_g curve	`C` parameter of surface phonon mobility degradation term	Depends on process conditions and other parameters – no validity range known	The extraction requires mostly an iteration between steps B and C and, sometimes, even between steps B, C, and D. Interface properties and material composition at the interface can change when changing process conditions. Fine-tuning is always necessary to fit I_d–V_g characteristics.
D	Transition between logarithmic and linear slope – threshold voltage region	1. Parameters of 2D Coulomb mobility degradation term 2. Parameters of InterfaceCharge model	1. No validity range known 2. No validity range known	Calibration focuses on the Coulomb roll-off visible in the $\mu(E_{\text{eff}})$ curve, but it also can be done to the bending of the I_d–V_g curve between subthreshold and linear region. These mobility degradation terms also affect the threshold voltage and the DIBL of the device.
E	Subthreshold region	Parameters of InterfaceCharge model	No validity range known	Calibration focuses on the Coulomb roll-off visible in the $\mu(E_{\text{eff}})$ curve, but it also can be done to the subthreshold region. This mobility degradation term also affects the threshold voltage and the drain-induced barrier lowering (DIBL) of the device.

Parasitic Series Resistance Extraction at Low Drain Bias

With the inclusion of a ballistic mobility model that gives a finite resistance for an infinitely small channel length, the calibration of the channel mobility is coupled to the calibration of the source/drain channel series resistance. Therefore, the extraction or determination of this series resistance is of utmost importance for the calibration of the parameters of the ballistic mobility model. Iterations might be needed to update the extracted series resistance when changing parameters of the ballistic mobility model in the calibration of the channel mobility.

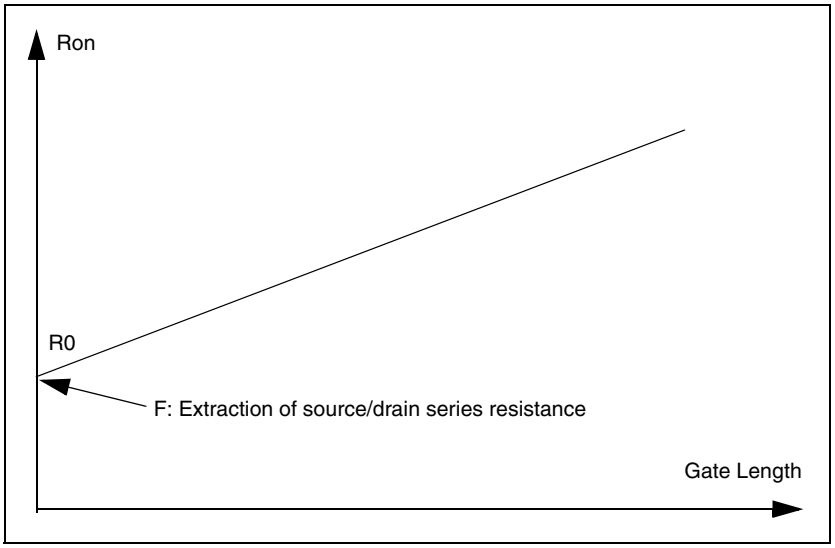

Figure 5 Extraction methodology of source/drain series resistance

Eq. 1 shows the parameters `R0` and `Rs` forming the on-resistance:

$$R_{\text{on}} = R0 + Lg \cdot Rs \tag{1}$$

Short-Channel Id–Vg Calibration at Low Drain Bias

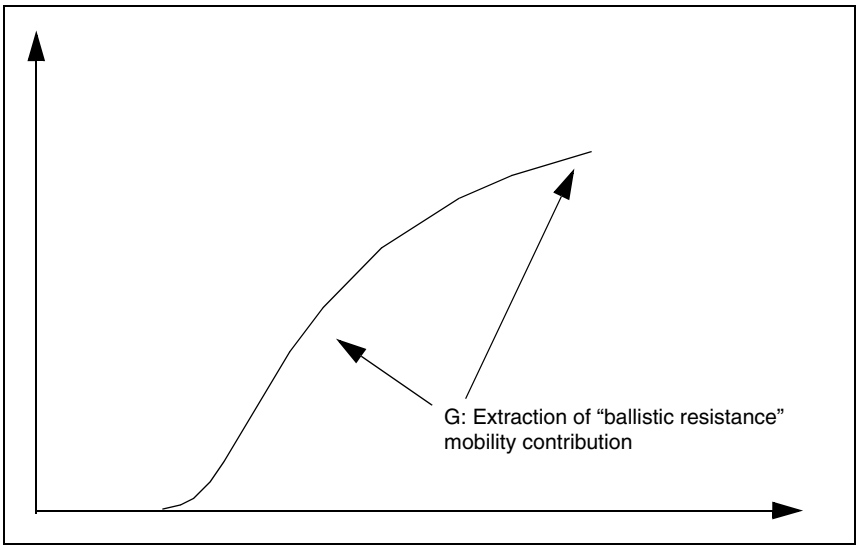

Figure 6 Short-channel I_d–V_g calibration methodology (linear scale, low drain bias voltage)

Table 7 Short-channel I_d–V_g calibration for low drain bias voltage

Step	Target	Parameter to extract	Validity range of parameter	Comments
G	Moderate and strong inversion	Adjust “ballistic resistance” mobility contribution using parameters of the ballistic mobility models in Sentaurus Device.	No validity range	Iteration with F.

Reference [1] discusses a possible overestimation of the current response close to equilibrium when having strong electrical built-in fields, for example, caused by p-n junctions. This effect might be connected to deviations from the Einstein relation in certain situations but is currently not considered in the calibration procedure because of convergence issues. This also means, to some extent, that the calibration of the parameters of the ballistic mobility model includes this physically different effect.

Short-Channel Id–Vg Calibration at High Drain Bias

In this step, saturation velocity is extracted.

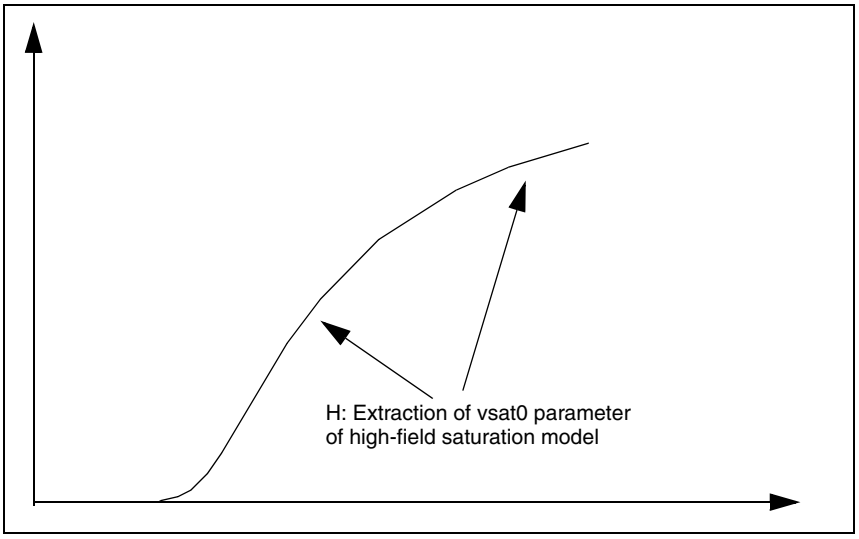

Figure 7 Short-channel I_d–V_g calibration methodology (linear scale, high drain bias voltage)

Table 8 Short-channel I_d–V_g calibration for high drain bias

Step	Target	Parameter to extract	Validity range of parameter	Comments
H	Whole I_d–V_g curve and I_{dsat}	Adjust `vsat0`	For silicon: < 5e7 cm/s	Iteration with F and G might be necessary.

The extraction of `vsat0` from I_{dsat} roll-off data or I_d–V_g curves at large drain bias voltage, using experiments or Monte Carlo (MC) simulation, is mostly straightforward. However, the calibration of both I_{dsat} and I_{dlin} at the same time using `vsat0`, source/drain resistance, and ballistic mobility parameters is more challenging. Nevertheless, it is mostly possible to achieve a good agreement during the device calibration because of the inclusion of the ballistic mobility model [2].

References

[1] A. T. Pham, C. Jungemann, and B. Meinerzhagen, “Modeling and validation of piezoresistive coefficients in Si hole inversion layers,” *Solid-State Electronics*, vol. 53, no. 12, pp. 1325–1333, 2009.

[2] A. Erlebach, K. H. Lee, and F. M. Bufler, “Empirical Ballistic Mobility Model for Drift-Diffusion Simulation,” in *Proceedings of the 46th European Solid-State Device Research Conference (ESSDERC)*, Lausanne, Switzerland, pp. 420–423, September 2016.

CHAPTER 5 Review of Models

This chapter provides a review of selected models of Sentaurus Device.

Overview of Models

Given the large number of different models developed and implemented in Sentaurus Device for the simulation of device characteristics, it is often difficult to quickly design appropriate command files for device simulation. Therefore, this chapter presents a review of selected models, and the models are evaluated with respect to their capabilities in simulating certain device aspects.

In the quantum drift-diffusion (QDD) approximation, charge carrier transport is determined by the electron and hole mobilities. Version N-2017.09 of Advanced Calibration Device focuses on low-field mobility and high-field mobility, with and without mechanical stress, for planar and nonplanar silicon and SiGe FETs. A discussion of models and parameters for InGaAs, AlGaN, and SiC devices is presented as well.

CMOS Devices

Unstrained Band Structure and Electrostatics

In Sentaurus Device, the bulk band structure is defined by the band gap, the electron affinity, the bandgap narrowing, and the density-of-states (DOS). The temperature dependency of these quantities and the doping dependency of the bandgap narrowing are represented by empirical functions.

Strained Band Structure and Electrostatics

The band structure changes with the mechanical stress in the device. The dependency of the conduction and valence bands and, therefore, of the band gap and electron affinity, on the mechanical stress or strain is described by the deformation potential model where the band structure information comes from $k \cdot p$ calculation. The stress dependency of the DOS can be extracted from $k \cdot p$ calculation as well.

Unstrained Low-Field Mobility

In the limit of low-driving fields, the mobility is degraded by several mechanisms. Typically, MISFET simulation takes into account mobility degradation by ionized dopants, surface roughness, surface phonon, and bulk phonon scattering. For high-k gate stacks, additional remote scattering mechanisms such as remote Coulomb scattering (RCS), remote phonon scattering (RPS), and remote dipole scattering (RDS) must be considered. A crucial point is the transition between bulk mobility and inversion or accumulation layer mobility. Because of the transition from 3D to 2D charge carrier gas, the scattering behavior of electrons and holes changes and screening becomes different. Furthermore, the mobility model must include the dependency on the channel material, which means for example on the germanium mole fraction, and on the channel and surface or interface orientations. For thin silicon films in the range of a few nanometers, additional contributions come into effect that cause a dependency of the mobility on the film thickness.

In summary, a drift-diffusion or QDD low-field mobility model for the simulation of SiON/SiO_2 or high-k gate stack FETs without mechanical stress should have the following features:

- Mobility degradation by ionized impurities – impurity Coulomb scattering (ICS)
- Mobility degradation by the roughness of the surface or interface – surface roughness scattering (SRS)
- Mobility degradation by interaction with bulk phonons – bulk phonon scattering (BPS)
- Mobility degradation by interaction with surface phonons – surface phonon scattering (SPS)
- Mobility degradation by charges in the gate isolator (high-k gate stack) (RCS)
- Mobility degradation by different permittivity in the gate isolator (high-k gate stack) (RPS)
- Mobility degradation by dipole configurations in the gate isolator (high-k gate stack) (RDS)
- Mole fraction dependency of the low-field mobility model parameters (for example, alloy scattering)
- Transition between bulk scattering and scattering in 2D charge carrier gas for ICS
- Parameters for different channel and surface or interface orientations (channel: <100> and <110>; surface: (100) and (110))
- Mobility degradation for very thin silicon films
- Including influence of quantization on mobility in thin films

Sentaurus Device offers low-field mobility degradation models for MISFET simulation:

- Bulk phonon-limited mobility model (BPS):

```
Physics { ConstantMobility }
```

- Mobility degradation by ionized impurities (in some cases, it contains, in the low-doping limit, the bulk phonon-limited mobility) (ICS):
  - Masetti model: Provides mole fraction–dependent model parameters:

```
Physics { Mobility ( DopingDependence (Masetti) ) }
```

  - Arora model: Provides mole fraction–dependent model parameters:

```
Physics { Mobility ( DopingDependence (Arora) ) }
```

  - Philips unified mobility model (`PhuMob`): Includes screening and carrier–carrier scattering, and provides mole fraction–dependent model parameters:

```
Physics { Mobility (PhuMob) }
```

  - University of Bologna bulk mobility model: Specially calibrated for an extended temperature range and provides mole fraction–dependent model parameters:

```
Physics { Mobility ( DopingDependence (UniBo2) ) }
```

  - Carrier–carrier scattering models (Conwell–Weisskopf and Brooks–Herring):

```
Physics { Mobility (CarrierCarrierScattering) }
```

- Mobility degradation at interfaces:
  - Enhanced Lombardi model: Includes automatic detection of surface orientation and provides mole fraction–dependent model parameters:

```
Physics { Mobility ( Enormal (Lombardi) ) }
```

  - Inversion and accumulation layer mobility model (`IALMob`): Includes automatic detection of surface orientation, provides mole fraction–dependent model parameters, and contains Philips unified mobility model, enhanced Lombardi model, and additional terms for Coulomb scattering in 2D electron gas:

```
Physics { Mobility ( Enormal (IALMob) ) }
```

  - University of Bologna surface mobility model: Specially calibrated for an extended temperature range, includes screening of bulk ICS, no special model for ICS in 2D charge carrier gas, simplified Lombardi-style model for acoustic phonon and surface roughness scattering:

```
Physics { Mobility ( Enormal (UniBo) ) }
```

- 2D Coulomb scattering model for ionized impurities: Must not be used together with `PhuMob` or any other `DopingDependence` model because mobility degradation is double counted; designed for Coulomb scattering (ICS) in 2D charge carrier gas:

  ```
  Physics { Mobility ( Enormal (Lombardi Coulomb2D) ) }
  ```

- 2D Coulomb scattering models for positive and negative charges at remote interfaces: Gives the possibility to distinguish between RCS and RDS:

  ```
  Physics { Mobility ( Enormal (Lombardi NegInterfaceCharge
     PosInterfaceCharge) ) }
  ```

- Thin-layer mobility model (`ThinLayer`): Describes mobility degradation due to finite silicon film thickness, includes dependency of phonon scattering on quantization but also additional empirical mobility degradation terms, and includes automatic detection of surface orientation. The model can be combined with `Enormal`-like models:

  ```
  Physics { Mobility (ThinLayer) }
  ```

Because of the use of Mathiessen's rule, several combinations of the above mobility models are possible. For MISFETs, you usually need to combine bulk phonon and Coulomb scattering with scattering at interfaces and surfaces. Historically, the following combinations have been used:

1. `DopingDependence(Masetti)` + `Lombardi`
2. `PhuMob` + `Lombardi`
3. `IALMob`
4. `IALMob` + `RPS` + `NegInterfaceCharge` + `PosInterfaceCharge`
5. `RPS` + `NegInterfaceCharge` + `PosInterfaceCharge` + `ThinLayer(IALMob)`

Model combination 2 has been used for a long time as the standard model. However, several problems call for a change to another low-field mobility model. First, the transition between 3D bulk Coulomb scattering and Coulomb scattering in the inversion layer is not correctly described because the `PhuMob` model, which is a bulk model, is used for the mobility degradation by scattering at ionized impurities from accumulation to strong inversion. This causes problems in describing the onset of the moderate or strong inversion around the threshold voltage in the I_d–V_g curve. Second, in thin silicon layers, it is mandatory to include the dependency on the film thickness.

NOTE For these reasons, it is necessary to change the low-field mobility framework and to switch to model combination 3, 4, or 5. The recommended models for MISFET simulation are model 3 (devices without high-k gate stacks), model 4 (devices with high-k gate stacks), and model 5 (thin films).

Strained Low-Field Mobility

Influence of Mechanical Stress

The modeling of the stress influence on the channel mobility must deal with several typical configurations. These configurations must be simulated accurately with the goal to minimize additional device calibration. The typical cases are:

- Planar silicon channel PMOS with compressive stress between 0.5 GPa and 2 GPa in the channel direction and up to 2 GPa tensile stress normal to the silicon surface (gate-first with SiGe pockets and dual stress liner (DSL)).
- Planar silicon channel PMOS with compressive stress between 1 GPa and 3 GPa in the channel direction and less than 500 MPa normal to the silicon surface (gate-last with SiGe pockets).
- Planar silicon channel NMOS with tensile stress between 1 GPa and 2 GPa in the channel direction and less than 500 MPa normal to the silicon surface (gate-last with SiC pockets).
- Planar silicon channel NMOS with tensile stress between 300 MPa and 1.5 GPa in the channel direction and up to 2 GPa compressive stress in the normal direction (gate-first with DSL and stress memorization technique).
- Planar PMOS channel with biaxial strained SiGe channel and stress between 1 MPa and 4 GPa in the channel direction and up to 2 GPa tensile stress in the normal direction (gate-first with DSL and SiGe pockets).
- Nonplanar silicon channel NMOS (FinFET) with mixed compressive or tensile stress components of up to 2 GPa depending on the configuration (for example, with SiC pockets wrapped around the fin and metal gate as a liner replacement).
- Nonplanar silicon channel PMOS (FinFET) with mixed compressive or tensile stress components of up to 2 GPa depending on the configuration (for example, with SiGe pockets wrapped around the fin and metal gate as a liner replacement).
- Nonplanar SiGe or Ge channel NMOS (FinFET) with mixed compressive or tensile stress components of up to 4 GPa depending on the configuration.
- Nonplanar SiGe or Ge channel PMOS (FinFET) with mixed compressive or tensile stress components of up to 4 GPa depending on the configuration.

The stress configurations must be simulated for several wafer orientations (for example, (001) and (1$\underline{1}$0)), channel directions (for example, <100> and <110>), and channel materials (for example, silicon and SiGe). Typically, all three stress components s_{xx}, s_{yy}, and s_{zz} are important. A model validity check, which is limited to uniaxial or biaxial stress configurations, is not sufficient. In addition, the response of the mobility degradation components (such as phonon scattering, Coulomb scattering, and remote scattering) to mechanical stress is different and requires the separate treatment of each component.

Typically, in Sentaurus Device, the total mobility is scaled with a stress enhancement factor calculated with the models discussed here. The models describing the influence of stress on the mobility available in Sentaurus Device are:

- First-order (linear) piezoresistance mobility model
- Second-order piezoresistance mobility model
- Nonlinear piezoresistance model for electrons and holes (`MCmob` and `SBmob`)
- Intel stress-induced hole mobility model (`hSixBand`)
- `eSubband` model for electrons
- `hSubband` model for holes

Several additional options can be chosen. For the piezoresistance models, the `Kanda` option includes the dependency of the stress-induced mobility change on the doping concentration. Differences in the influence of mechanical stress on minority and majority carriers can be considered by an additional fitting parameter. In addition, you can calibrate the influence of the normal electric field in a MIS structure and of the germanium mole fraction on the first-order piezo coefficients. Because the linear piezoresistance model is a bulk model, the default piezoresistance coefficients are not accurate for inversion layers and must be adjusted. The piezoresistance model can be used as a factor model or a tensor model, in this way, introducing anisotropic properties.

The influence of the saturation velocity on the stress-dependent mobility can be fine-tuned by a parameter that controls how strongly the saturation velocity depends on the stress. Setting this parameter to zero means the mobility change is applied to the low-field mobility only. Setting the parameter to 1, which is the default in Sentaurus Device, means the mobility change is applied to the total mobility. Because it is known from MC simulation and from experiments that short-channel transistors show a much lower mobility enhancement due to mechanical stress, it is better to apply the mobility change to the low-field mobility only. Further adjustment of this parameter should be performed with good references only.

The occupation-based and band structure–based models (`eSubband` and `hSubband` models, and Intel model) have their own dependency on the doping concentration, and a `Kanda`-like option is not necessary. In addition, the electric field dependency should be a result of the model itself.

The following sections describe the models and options, and give some information about problems and advantages.

Piezoresistance Mobility Models

First-Order (Linear) Piezoresistance Mobility Model

This model uses the piezoresistance tensor with constant coefficients to calculate the stress-induced mobility change.

Options:

It can be used as a factor (isotropic) model or a tensor (anisotropic) model. The piezoresistance coefficients can depend on the normal electric field in an inversion layer. Minority and majority charge carrier transport can be distinguished. Dependency on the doping concentration can be included. Calibration of dependency of the influence of mechanical stress on the velocity saturation is possible.

Advantages:

The model is well adjusted to measurements for the bulk case. It is fully transformable, making it possible to consider all stress configurations and current directions in a bulk situation. It is easy to use and to calibrate.

Problems:

Accurate for low stress only (< 200 MPa). Tensor symmetry is broken for nonbulk conditions as in an inversion layer, which is not reflected by the model. Default piezoresistance coefficients are not accurate for inversion layers.

Second-Order Piezoresistance Mobility Model

This model uses the 6th-grade piezoresistance tensor with constant coefficients to calculate the stress-induced mobility change.

Options:

The model can be used as a factor (isotropic) model or a tensor (anisotropic) model. Minority and majority charge carrier transport can be distinguished. Dependency on the doping concentration can be included. Calibration of dependency of the influence of mechanical stress on the velocity saturation is possible.

Advantages:

Parameters are available for the bulk case. The model is fully transformable, making it possible to consider all stress configurations and current directions in a bulk situation.

Problems:

Accurate for low and moderate stress values only (< 500 MPa). Tensor symmetry is broken for nonbulk conditions as in an inversion layer, which is not reflected by the model. Default piezoresistance coefficients are not accurate for inversion layers.

Nonlinear Piezoresistance Models for Electrons and Holes (MCmob and SBmob)

These models can use nonlinear piezoresistance coefficients and higher-order cross-term corrections that are extracted from MC simulation, Sentaurus Band Structure simulation, or other sources (experiments and simulations available from the literature).

Options:

Minority and majority charge carrier transport can be distinguished. Dependency on the doping concentration can be included. Calibration of dependency of the influence of mechanical stress on the velocity saturation is possible. Germanium mole fraction dependency of the model coefficients can be switched on. Parameters for different orientations can be used and an auto-orientation option is available. Complete parameter sets can be loaded using the Sentaurus Device parameter file.

Advantages:

Parameters are available for strong inversion and for different channel materials (silicon and SiGe). The model can be extended to other conditions when there are reference tools such as MC simulations or experiments. Available for different channel and wafer orientations. The model is fast and can be calibrated easily.

Problems:

Interpolation especially for untypical stress conditions must always be validated. The physics is in the reference tool, for example, the MC simulator. Improvement of the model without improving the reference tool or without obtaining better experiments is, except with respect to the interpolation, not possible. The settings for the local coordinate system must be specified in the Sentaurus Device parameter file.

Occupation-Based and Band Structure–Based Models

The models in this section characterize the dependency of occupation and band structure on mechanical stress for the calculation of the mobility.

Intel Stress-Induced Hole Mobility Model (hSixBand)

This model uses the change of band structure and occupation to calculate stress-dependent mobility.

Options:

Dependency on the doping or carrier concentration can be switched on.

Advantages:

The model is derived from physical assumptions.

Problems:

Calibration is not straightforward. Only silicon as a channel material is available. The influence of surface orientation cannot be described. The model has been developed and calibrated for uniaxial stress in the <110> direction. The combination of the component normal to the MIS plane with the in-plane stress components is not validated.

eSubband Model for Electrons

This model uses a change of band structure and occupation to calculate the mobility change.

Options:

Dependency on the doping or carrier concentration can be switched on. Stress-related change in the scattering can be included. Change of effective mass with stress can be added to the model. For the inversion layer, the `MLDA` option can be used.

Advantages:

The modified local-density approximation (MLDA) allows you to move from bulk to inversion layer conditions, and to take surface or channel orientation dependency into account. The model is derived from physical assumptions. The model is validated and calibrated for silicon and SiGe for different channel and surface orientations. Mole fraction dependency for SiGe is available.

Problems:

Calibration is not straightforward.

hSubband Model for Holes

This model uses a change of band structure and occupation to calculate stress-dependent mobility.

Options:

Dependency on the doping or carrier concentration can be switched on. Stress-related change in the scattering can be included. Change of effective mass with stress can be added to the model. For the inversion layer, the `MLDA` option can be used.

Advantages:

MLDA allows you to move from bulk to inversion layer conditions, and to take surface or channel orientation dependency into account. The model is derived from physical assumptions. The model is validated and calibrated for silicon and SiGe for different channel and surface orientations. Mole fraction dependency for SiGe is available.

Problems:

Calibration is not straightforward.

Unstrained High-Field Mobility

The low-field mobility models are valid for small driving forces only. To take into account high-field effects, an additional model – the high-field saturation model – is introduced in the drift-diffusion model framework. The high-field saturation model should limit the velocity-field relation to the saturation velocity of the material when having sufficient scattering, and it must provide a way to calibrate the influence of quasiballistic and ballistic transport on the charge carrier transport. In addition, it should give the possibility to calibrate the germanium mole fraction dependency of the model parameters. Furthermore, because of deficiencies in the drift-diffusion model to describe the current response close to equilibrium, a model is needed that gives the possibility to compensate or, at least, to calibrate for this deficiency.

In summary, a drift-diffusion or QDD high-field mobility model for the simulation of SiON/ SiO_2 or high-k gate stack FETs without mechanical stress should have the following features:

- For unstrained cases with sufficient scattering limitation of the drift velocity to the saturation velocity for high fields.
- Possibility to calibrate the model with respect to ballistic and quasiballistic transport.
- Germanium mole fraction–dependent model parameters.

- Possibility to calibrate the model with respect to current response close to equilibrium.
- Orientation-dependent model parameters.

Sentaurus Device offers high-field mobility models for MISFET simulation:

- Extended Canali model: It is the mainstream model for drift-diffusion simulation, and it can be used with the hydrodynamic model as well. It has calibrated parameters for silicon and SiGe for situations where ballistic or quasiballistic transport is not present. Calibration to short-channel devices where quasiballistic transport occurs can be done using model parameters:

  ```
  Physics { Mobility (HighfieldSaturation) }
  ```

- Transferred electron model: Specially designed for GaAs and materials with similar band structure:

  ```
  Physics { Mobility ( HighfieldSaturation (TransferredElectronEffect) ) }
  ```

- Basic model: Simple model with carrier temperature as the driving force and requires the hydrodynamic model:

  ```
  Physics { Mobility ( HighfieldSaturation (CarrierTempDriveBasic) ) }
  ```

- Meinerzhagen–Engl model: Canali-like high-field saturation model with carrier temperature as the variable and requires the hydrodynamic model:

  ```
  Physics { Mobility ( HighfieldSaturation (CarrierTempDriveME) ) }
  ```

The common model for drift-diffusion or QDD simulations is the extended Canali model.

NOTE Calibrated mole fraction–dependent parameters are available and extensive experience exists. Numeric problems are known or are already solved.

Strained High-Field Mobility

The dependency of the high-field mobility on mechanical stress is determined, in the QDD model, by the strain dependency of the saturation velocity. The saturation velocity covers in this model both the strain dependency of the physical saturation velocity and the strain dependency of the quasiballistic transport. The model is again the Canali model where the parameter `saturationfactor` controls the stress dependency.

Gallium Nitride HEMTs

GaN HEMTs have unique qualities that require special attention. First, there is the large band gap that results in very low charge-carrier densities as well as numeric problems. Second, in the on-state, the current conduction is performed using a 2D electron gas channel in the GaN layer. This has implications for the modeling of the mobility. Third, most of these structures use material combinations in addition to pure GaN and AlN such as AlGaN. The mole fraction of these alloys determines the thermal conductivity, mobility, and band gap. For that, mole fraction–dependent parameters that make the transition from GaN to AlN are necessary. Mostly, linear or parabolic interpolation between GaN and AlN is not sufficient because of the alloy influence. Furthermore, there is the influence of the strain causing polarization in the device. In addition, traps heavily influence the device operation, and the velocity saturation behavior is different to silicon.

Silicon Carbide Devices

As another wide bandgap material, SiC shows some differences to silicon as well. There are again numeric problems connected with the small densities caused by the large band gap. The anisotropy of the mobility and of the avalanche coefficients is difficult to handle numerically. Traps, contact behavior, incomplete ionization, and tunneling play more critical roles than in silicon devices.

Because of the wide band gap, the incomplete ionization model (`IncompleteIonization`) must be included in the simulation. Anisotropic behavior can be considered for thermal conductivity, mobility, and impact ionization.

Silicon Smart-Power Devices

The model requirements are similar to those for silicon deep-submicron devices (see Chapter 3 on page 5) fabricated by gate-first processes, but with a greater variety of process and doping conditions as well as layout specifications. In addition, there is a need for:

- High accuracy over a wide temperature range up to very high temperatures.
- Good modeling capabilities for avalanche and breakdown.
- Good modeling capabilities for electrostatic discharge (ESD).

For avalanche, the new University of Bologna impact ionization model (`UniBo2`) is calibrated for a temperature range from 300 K to 773 K and is, therefore, best suited for ESD and high-temperature simulations. It also is recommended for room-temperature breakdown simulations.

CHAPTER 6 Parameter Files

This chapter discusses the features of the parameter files.

The information presented here relates to the models presented in Chapter 3 on page 5 and to the files that are stored in the `MaterialDB` folder of Sentaurus Device.

Content of Parameter Files of Advanced Calibration Device

The `Silicon.par`, `Germanium.par`, `SiliconGermanium.par`, `Siliconc110.par`, `Siliconc100.par`, `SiliconGermaniumc110.par`, or `SiliconGermaniumc100.par` file must be loaded when simulating silicon or SiGe CMOS or silicon smart-power devices.

The `AlN.par`, `AlGaN.par`, `GaN.par`, `InGaN.par`, `AlInGaN.par`, `InN.par`, and `AlInN.par` files must be loaded when simulating wide-bandgap III–V nitride devices. The `SiliconCarbide.par`, `4H-SiC.par`, or `6H-SiC.par` file must be loaded when simulating SiC devices.

The `InAs.par`, `InGaAs.par`, and `GaAs.par` files must be loaded when simulating III–V–arsenide devices.

Table 9 on page 40 lists the content and the features of the parameter files. The references and additional comments for the parameters can be found in the parameter files.

Table 9 Content and features of parameter files

Parameter file	Material	Parameters for...
`GaN.par`	GaN	• Isotropic and anisotropic permittivity • Thermal conductivity • Lattice heat capacity • Band gap and affinity • Density-of-states (DOS) • Mobility with doping dependency • High field dependency • Shockley–Read–Hall (SRH) • Auger • Radiative recombination • Impact ionization • Piezoelectric polarization • Optical material properties • Mechanical compliance parameters
`AlN.par`	AlN	• Isotropic and anisotropic permittivity • Thermal conductivity • Lattice heat capacity • Band gap and affinity • DOS • Mobility with doping dependency • High field dependency • SRH • Auger • Impact ionization • Piezoelectric polarization • Optical material properties • Mechanical compliance parameters
`AlGaN.par`	AlGaN	• For most of the models, the mole fraction dependency is linearly interpolated between the corner materials GaN and AlN • U-shape of thermal conductivity is described by a piecewise linear spline function in the parameter file • Mole fraction–dependent band gap (parabolic interpolation) • Mole fraction–dependent mobility with doping dependency is described by a piecewise linear spline function in the parameter file • Mole fraction–dependent high field dependency is described by a piecewise linear spline function in the parameter file • Mole fraction–dependent impact ionization is described by a piecewise linear spline function in the parameter file • Mole fraction–dependent piezoelectric polarization • Mechanical compliance parameters

Table 9 Content and features of parameter files

Parameter file	Material	Parameters for...
`InGaN.par`	InGaN	• For most of the models, the mole fraction dependency is linearly interpolated between the corner materials GaN and InN.
`AlInGaN.par`	AlInGaN	• For most of the models, the mole fraction dependency is linearly interpolated between the corner materials AlN, GaN, and InN.
`AlInN.par`	AlInN	• For most of the models, the mole fraction dependency is linearly interpolated between the corner materials AlN and InN.
`InN.par`	InN	• Isotropic and anisotropic permittivity • Thermal conductivity • Lattice heat capacity • Band gap and affinity • DOS • Mobility with doping dependency • High field dependency • Impact ionization • Piezoelectric polarization • Mechanical compliance parameters

`SiliconCarbide.par`
`4H-SiC.par`
`6H-SiC.par`
	SiC	• Isotropic and anisotropic permittivity
		• Isotropic and anisotropic thermal conductivity
		• Lattice heat capacity
		• Band gap and bandgap narrowing
		• DOS
		• Mobility with doping dependency
		• Anisotropic mobility
		• Isotropic and anisotropic high field dependency
		• SRH
		• Auger
		• Isotropic and anisotropic impact ionization
		• Incomplete ionization

`Silicon.par`
`Siliconc100.par`
`Siliconc110.par`
	Si	• Permittivity
		• Thermal conductivity
		• Band gap and bandgap narrowing
		• DOS
		• Quantization
		• Bulk and inversion mobility for different surface and channel orientations, and film thicknesses
		• High field dependency
		• Other model parameter sections are available in the parameter file but are not yet updated and reviewed

Table 9 Content and features of parameter files

Parameter file	Material	Parameters for...

`SiliconGermanium.par`
`SiliconGermaniumc100.par`
`SiliconGermaniumc110.par`
	SiGe (0–100%) can be used for Ge as well	• All models are mole fraction dependent
		• Permittivity
		• Thermal conductivity
		• Band gap and bandgap narrowing
		• DOS
		• Quantization
		• Bulk and inversion mobility for different surface and channel orientations, and film thicknesses
		• High field dependency
		• Other model parameter sections are available in the parameter file but are not yet updated and reviewed

`Germanium.par`	Germanium	• Permittivity • Thermal conductivity • Band gap and bandgap narrowing • DOS • Bulk mobility • High field dependency • Optical properties • Other model parameter sections are available in the parameter file but are not yet updated and reviewed
`InGaAs.par`	InGaAs	• Permittivity • Heat capacitance • Thermal conductivity • Band structure (band gap, affinity) • Bandgap narrowing • DOS • Bulk and inversion mobility for different surface and channel orientations • Quantization parameters • Optical properties • Other model parameter sections are available in the parameter file but are not yet updated and reviewed
`InAs.par`	InAs	• Permittivity • Heat capacitance • Thermal conductivity • Band structure (band gap, affinity) • Bandgap narrowing • DOS • Bulk and inversion mobility for different surface and channel orientations • Quantization parameters • Optical properties • Other model parameter sections are available in the parameter file but are not yet updated and reviewed

Table 9 Content and features of parameter files

Parameter file	Material	Parameters for...
GaAs.par	GaAs	• Permittivity • Heat capacitance • Thermal conductivity • Band structure (band gap, affinity) • Bandgap narrowing • DOS • Bulk and inversion mobility for different surface and channel orientations • Quantization parameters • Optical properties • Other model parameter sections are available in the parameter file but are not yet updated and reviewed

Special Parameter Files

In the MaterialDB folder of Sentaurus Device, there are special parameter files that reflect certain application cases. These files are stored in the directory custom in the MaterialDB folder, and they are:

```
GatePolySilicon.par
mcmob.par
sbmob.par
StrainedSi_SiGe.par
SiGeHBT.par
StrainedSilicon.par
```

The GatePolySilicon.par file is a parameter file for the polysilicon gate of FETs. The mcmob.par and sbmob.par parameter files contain the default parameter set for the MCmob and SBmob PMI models.

The parameter file StrainedSi_SiGe.par contains in-plane transport parameters at 300 K for silicon under biaxial tensile strain present when a thin silicon film is grown on top of a relaxed SiGe substrate (*in-plane* refers to charge transport that is parallel to the interface to SiGe as is the case for MOSFETs). This parameter file defines parameters for the materials StrainedSilicon, Silicon, and Oxide. Further explanation can be found in the header of this parameter file.

The parameter file StrainedSilicon.par contains the same parameters as StrainedSi_SiGe.par for a strained Silicon material, but it does not contain the corresponding material sections for Silicon and Oxide.

The `SiGeHBT.par` parameter file contains transport parameters at 300 K for SiGe under biaxial compressive strain present when a thin SiGe film is grown on top of a relaxed silicon substrate, such as occurs in the base of npn-SiGe heterojunction bipolar transistors (HBTs). The electron parameters refer to the out-of-plane direction (that is, perpendicular to the SiGe–silicon interface) and the hole parameters refer to the in-plane direction (that is, parallel to the SiGe–silicon interface). The transport parameters have been obtained from full-band Monte Carlo simulations. Further explanation can be found in the header of the parameter file.

CHAPTER 7 Quality of Fitting and Extraction

This chapter discusses fitting quality and extraction issues.

Low-Field Mobility of Planar CMOS Devices With Silicon Channel

Oxide–Silicon Interface

This section briefly explains how the low-field mobility parameter sets were calibrated.

Data from Takagi *et al*. [1][2], Nakamura *et al*. [3], and Nayfeh *et al*. [4] was used for the calibration of the mobility in the transistor channel. All data is from pure polysilicon/SiO_2 gate stacks with oxide thicknesses of 25 nm for Takagi, 2 nm for Nakamura, and 5 nm for Nayfeh.

This data does not have high-k gate stacks and, therefore, allows you to extract the model parameters of surface phonon, surface roughness, and Coulomb scattering at ionized impurities. On the other hand, the process-induced variations in surface roughness and the material composition of the first atomic layers at the isolator–silicon interface can influence the mobility and result in different mobilities for different gate-formation process steps. These differences cannot be reflected by a single parameter set. Therefore, the parameter set presented here is a starting point for calibration.

Usually, the extraction of low-field mobility as a function of the effective electric field E_{eff} is performed in the following way.

First, the drain current is measured in the linear regime and, from that, the mobility is calculated for each gate voltage. At the same time, the inversion charge per area N_{inv} is calculated from C–V characteristics. Because E_{eff} is not measured, it must be calculated from N_{inv} using $E_{\mathrm{eff}} = E_{\mathrm{eff}}(N_{\mathrm{depl}}, N_{\mathrm{inv}}, \eta)$. Mostly, the depletion approximation with N_{depl} as the depletion charge is used for this, where the doping is extracted from other experiments and is assumed to be constant. The result is the dependency $\mu = \mu(E_{\mathrm{eff}})$. To obtain the universal behavior, that is, doping-independent behavior of the mobility for strong inversion, the fitting parameter η is introduced in the equation used for determining the effective field. You must use different values for η to obtain the universal behavior for different charge carriers and surface orientations (electrons: 1/2 for (100) and 1/3 for (110), holes: 1/3).

These standard parameters provide mostly good universal behavior for a (100) surface orientation and low to moderate doping. For a (110) surface orientation, high-doping, or nonplanar and double-gate devices, the universal behavior is mostly not fully achieved. In general, it remains a question of whether the use of this extraction method, and especially the use of the same η in the extraction from measurement and simulation, is correct.

If $\eta = 1$, E_{eff} corresponds exactly to the electric field at the interface in the depletion approximation. However, $\eta < 1$ lowers the field strength, thereby taking into account that the current flow is not only at the surface but also distributed a few nanometers into the depth of the silicon. Because it is not clear whether the field and current density distribution as well as the local dependency of the mobility on the electric field are described sufficiently in simulation, it may often be very difficult to achieve universal behavior in simulations with the same η parameter as in measurement.

In many cases, this universality is achieved only by introducing an artificial doping dependency for the surface phonon scattering (SPS) and the surface roughness scattering (SRS) in the Lombardi terms for the mobility models. However, it is not clear whether this doping dependency exists at all, or whether it is only a result of this forced parameter fitting. It can result in an unusual situation where the mobility degradation in intrinsic or very low–doped regions is actually stronger than in high-doped regions and drops to completely unrealistic values.

Because of this, another extraction methodology is used for the mobility parameters. The mobility model is calibrated to the measured $\mu = \mu(N_{\mathrm{inv}})$ curves. For this, no calibration of η is necessary, and universal behavior is not requested. After this, a check is performed with $\mu = \mu(E_{\mathrm{eff}})$ but additional calibration is performed only when there are strong disagreements. Figure 8 to Figure 16 show the agreement between measurement and simulation.

In simulating CMOS devices with precalibrated parameter sets, you must always take into account that the precalibrated parameter sets are *initial* parameter sets that can undergo additional fine-tuning and major changes. The reasons are mainly connected with the dependency of the mobility degradation on the processing.

For example, the interface or surface roughness depends on the process conditions and the materials involved. Applying the parameters extracted above to modern FinFET devices with <110> channel direction, you can see that the inversion mobility is often underestimated, which is connected to the fact that the surface roughness–related mobility degradation is smaller on the (110) fin sidewalls than in the planar (110) case [5].

Similarly, for the surface phonon–related interface mobility, the process conditions and the materials involved introduce some uncertainties that do not allow you to derive a parameter set that is valid for several device types or technology generations. Recalibration is mostly necessary.

The strength of RCS or RDS depends on the number of charges in the high-k gate stack and their position. The model must be calibrated to measurements when switching it on. RCS and RDS have the same origin: the mobility degradation by charges in the high-k gate stack. The difference is in the presence of both negative and positive charges in the case of RDS. For RPS, the parameters are extracted from MC simulation. Depending on the high-k gate stack properties, fine-tuning may be necessary. However, because it is difficult to extract the correct parameters without having mobility measurements for different interfacial layer thicknesses and different temperatures, it is recommended to keep the parameters and to focus on the calibration of RCS and RDS.

The Philips unified mobility model (`PhuMob`) is calibrated to bulk mobility measurements. Usually, fine-tuning is necessary only when performing custom calibration with high-accuracy requirements. In addition, the mobility fine-tuning cannot be separated from the doping concentration or dopant activation calibration. Therefore, it is recommended that you keep the default parameters. In the framework of the inversion and accumulation layer model (`IALMob`), when going to inversion layer conditions, 3D Coulomb scattering turns to 2D Coulomb scattering, the `PhuMob` model is switched off, and the 2D Coulomb scattering model takes over. The 2D Coulomb scattering model is a very simple description of reality with many fitting parameters. The influence of this model is mainly in the onset of the I–V curves. The default parameters are not very good. Additional calibration is necessary.

The stress dependency of the mobility resulting from `hSubband` (holes), `eSubband` (electrons), `MCmob`, and `SBmob` simulations has been compared to the literature and in-house Monte Carlo (Sentaurus Device Monte Carlo) and Kubo–Greenwood (Sentaurus Band Structure) simulations [6][7][8].

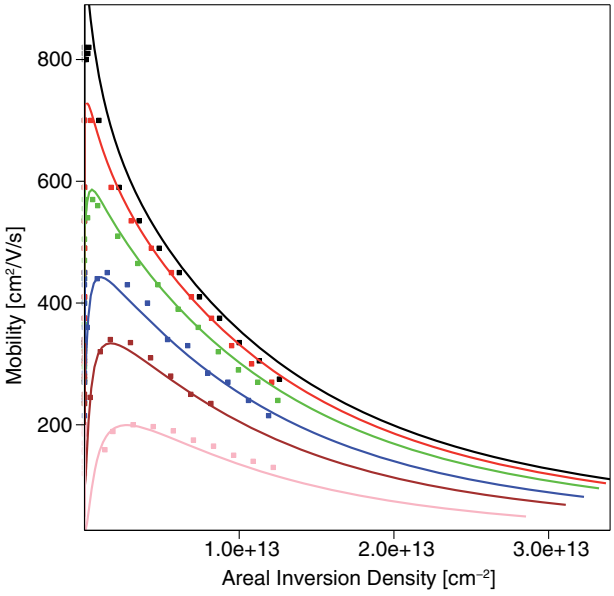

Figure 8 Electron mobility versus areal inversion density for (100) surface in linear scale (channel doping from top to bottom: 3.9e15, 2e16, 7.2e16, 3e17, 7.7e17, 2.4e18)

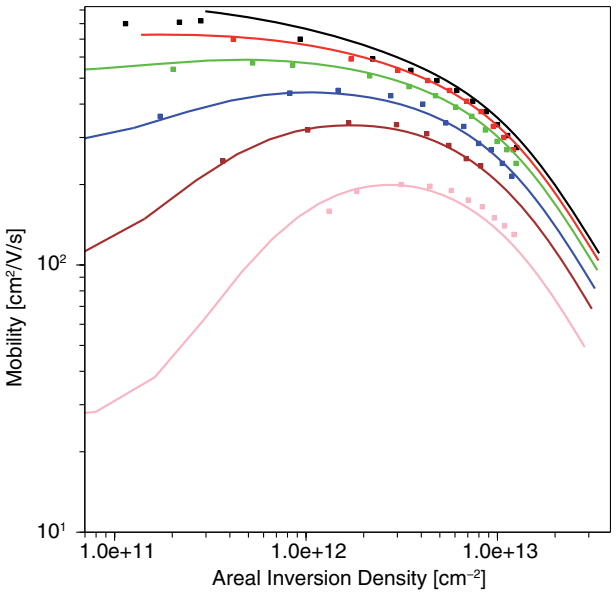

Figure 9 Electron mobility versus areal inversion density for (100) surface in logarithmic scale (channel doping from top to bottom: 3.9e15, 2e16, 7.2e16, 3e17, 7.7e17, 2.4e18)

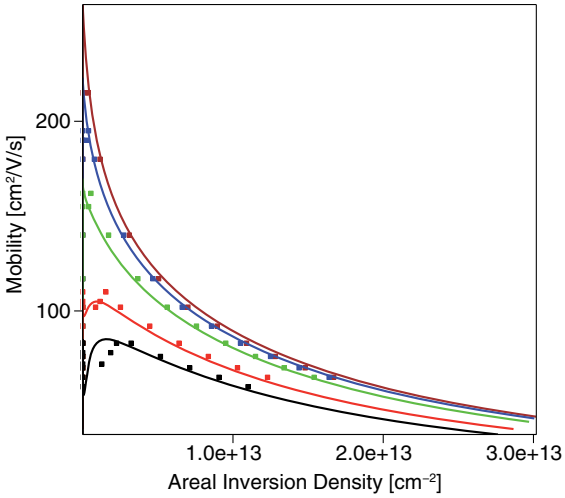

Figure 10 Hole mobility versus areal inversion density for (100) surface in linear scale (channel doping from top to bottom: 7.8e15, 1.6e16, 5.1e16, 2.7e17, 6.6e17)

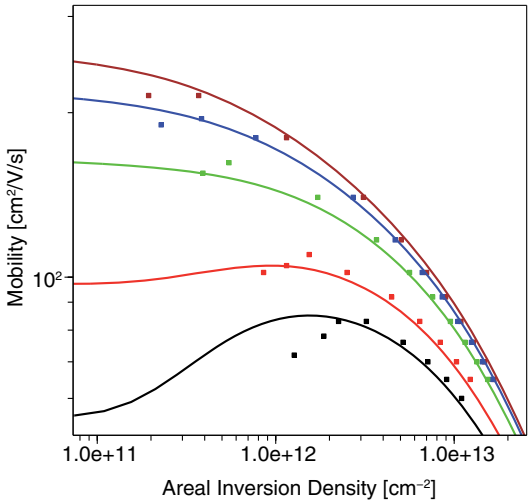

Figure 11 Hole mobility versus areal inversion density for (100) surface in logarithmic scale (channel doping from top to bottom: 7.8e15, 1.6e16, 5.1e16, 2.7e17, 6.6e17)

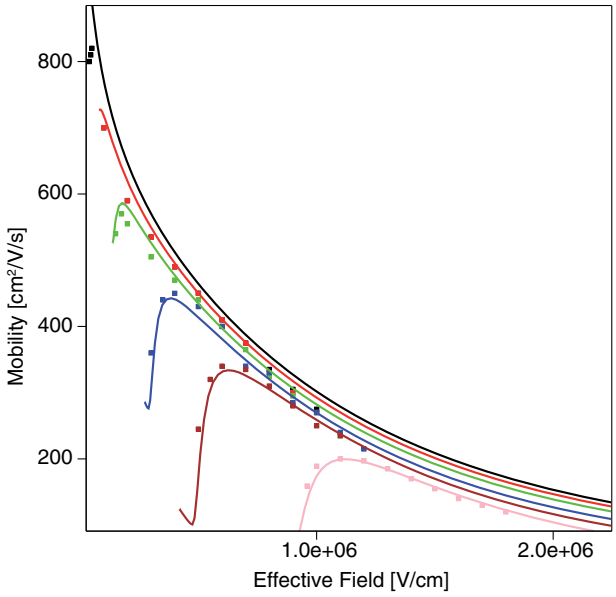

Figure 12 Electron mobility versus effective field for (100) surface in linear scale (channel doping from top to bottom: 3.9e15, 2e16, 7.2e16, 3e17, 7.7e17, 2.4e18)

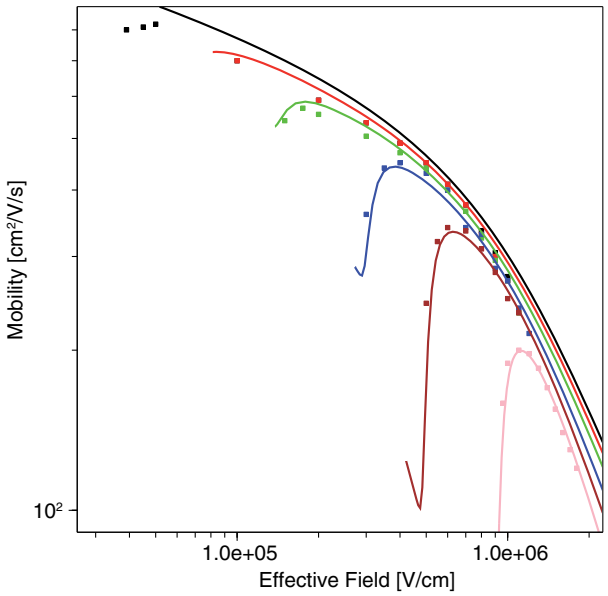

Figure 13 Electron mobility versus effective field for (100) surface in logarithmic scale (channel doping from top to bottom: 3.9e15, 2e16, 7.2e16, 3e17, 7.7e17, 2.4e18)

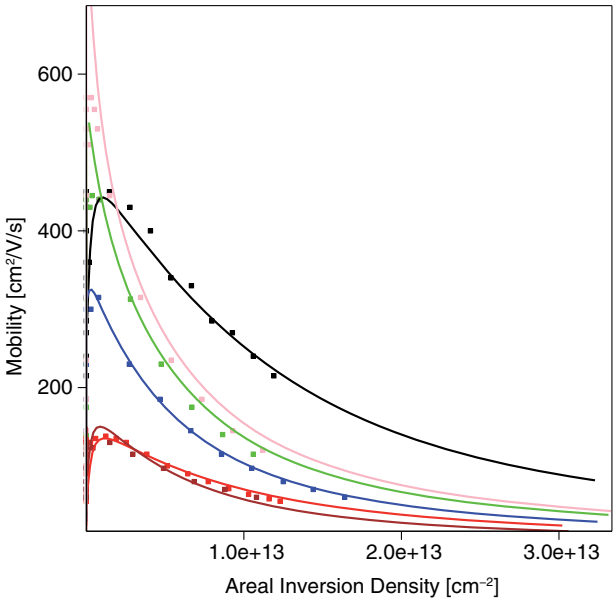

Figure 14 Electron mobility versus areal inversion density for (100) surface as a reference and for (110)/<100> and (110)/<110> in linear scale (channel doping between 5e17 and 9e17)

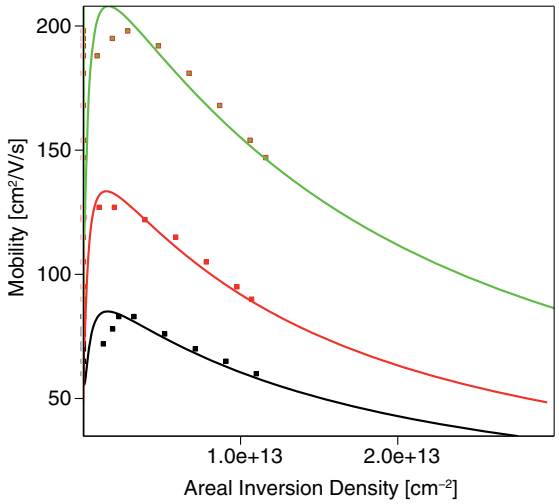

Figure 15 Hole mobility versus areal inversion density for (100) surface as a reference and for (110)/<100> and (110)/<110> in linear scale (channel doping between 4.5e17 and 6.6e17)

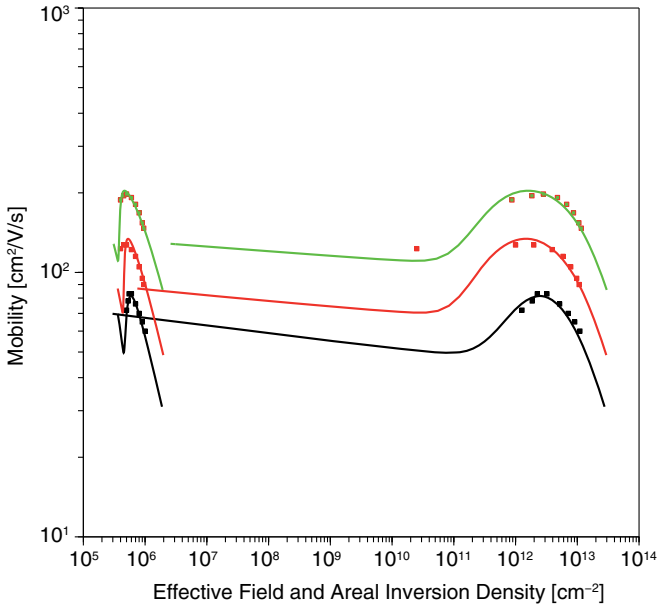

Figure 16 Hole mobility versus effective field and areal inversion density for (100) surface as a reference and for (110)/<100> and (110)/<110> in double logarithmic scale (channel doping between 4.5e17 and 6.6e17)

Influence of Metal Gate on Inversion Layer Mobility

The parameter set used to produce the results shown in Figure 8 to Figure 16 is derived from measurements on devices with a polysilicon/oxide gate stack. In devices with a metal/oxide gate stack, the channel mobility can be different because of the influence of the metal gate. The same holds for the comparison between polysilicon/HfO_2 and metal/HfO_2 gate stacks.

Usually, the transition from the polysilicon gate to the metal gate results in an improvement of the mobility. One reason for this could be the better screening of surface phonons and charges in the gate stack by the charge carriers in the metal gate [9]. Table 10 presents an overview of the influence of different gate materials on the inversion layer mobility.

Table 10 Influence of gate material on inversion layer mobility for electrons according to [9]

Gate stack	Maximum mobility [$cm^2/V/s$]	Mobility at E_{eff} = 1 MV/cm [$cm^2/V/s$]
HfO_2/Polysilicon	175	145
HfO_2/TiN	245	200

The increasing mobility caused by the metal gate can be reflected by an increase of the `IALMob` parameters `B`, `C`, and `delta` by a factor of 1.4.

Influence of High-k Gate Stack on Inversion Layer Mobility

The parameter set used to produce the results shown in Figure 8 to Figure 16 is derived from measurements on devices with a polysilicon/oxide gate stack. In devices with a high-k isolation, for example, with HfO_2, the channel mobility can be degraded because of the influence of charges in the gate isolator (remote Coulomb or dipole scattering (RCS or RDS)) and remote phonon scattering (RPS). Often, the charges are arranged in dipole-like configurations. The RCS-related mobility degradation depends on the number and the arrangement of the charges in the gate isolator, especially on their distance to the inversion layer. RCS depends greatly on the process conditions and the materials used in the gate stack, and so the variation between technologies and process splits and even over the wafer and between wafers can be large. Therefore, it is not possible to provide well-calibrated default parameters, but custom calibration to the process and device under consideration is mostly necessary. However, the model should be able to describe the major tendencies such as the dependency on the thickness of the interfacial oxide or on the concentration of charges in the gate stack.

Table 11 and Table 12 list a set of model parameters for the `InterfaceCharge` models and for the `RPS` model that fulfill these requirements.

Table 11 Recommended parameter values for RPS model

Parameter	Value	Comment
`l_crit` for electrons	7.7e-8 cm	[10]
`l_crit` for holes	7.7e-8 cm	[10]
`d_crit` for electrons	1.0e-7 cm	Distance between high-k interface and silicon interface.
`d_crit` for holes	1.0e-7 cm	Distance between high-k interface and silicon interface.
`murps0` for electrons	124 $cm^2/(Vs)$	Extracted from Sentaurus Device Monte Carlo simulation.
`murps0` for holes	124 $cm^2/(Vs)$	Extracted from Sentaurus Device Monte Carlo simulation.

Table 12 Recommended parameter values for InterfaceCharge models (RCS and RDS, NegInterfaceCharge and PosInterfaceCharge models use the same parameters)

Parameter	Values for electrons/holes	Comment
`E0`	1.0e-6 / 1.0e-6	
`mu1`	250 / 250	
`c_exp`	0.5 / 0.5	
`l_crit`	7.7e-8 / 7.7e-8	[10]

Extraction of Contact Resistance Parameters

The contact resistance between PtSi/NiSi and silicon has been measured by Stavitski *et al*. [11]. Based on this data, the parameters for the `SchottkyResist` model in Sentaurus Device are extracted and presented in Table 13 and Table 14 on page 54. No additional tests or validations have been performed with this parameter set. In addition, the parameters are currently not included in the `MaterialDB` parameter files.

Table 13 Parameters for SchottkyResist model for PtSi

Parameter	Values for electrons/holes
barrier	0.8 eV / 0.4 eV
Rinf	3.0e-10 $\Omega\,cm^2$ / 3.0e-10 $\Omega\,cm^2$
mt	0.08 / 0.08

Table 14 Parameters for SchottkyResist model for NiSi

Parameter	Values for electrons/holes
barrier	0.6 eV / 0.6 eV
Rinf	1.0e-9 $\Omega\,cm^2$ / 5.0e-10 $\Omega\,cm^2$
mt	0.08 / 0.08

Basic Properties of Silicon Carbide (SiC) Devices

The parameter values and the corresponding references also can be found in the parameter files `4H-SiC.par` and `6H-SiC.par` and in [12].

All SiC polytypes are indirect semiconductors, and the maximum of the upper valence bands is located at the center (Γ-point) of the Brillouin zone. Conduction band minima of 3C-SiC, 6H-SiC, and 4H-SiC are located at the points X, U on the (L-M) line, and M, respectively.

Photoluminescence or absorption measurements give an exciton band gap E_{gx}. There are no reliable measured values for binding energies E_x of free excitons, which are required to obtain the indirect band gap $E_g = E_{gx} + E_x$. As measured values of E_x range from 10–80 mV, a mean direct band gap may be assumed by shifting E_{gx} by 40 mV. In the parameter file, a value of `Eg0`=3.285 eV is finally used.

Temperature dependency of the band gap is measured for 6H-SiC in the temperature ranges from 6 K to 200 K, and from 300 K to 700 K. The dependency of 3C-SiC is measured in the temperature range from 295 K to 700 K. The respective dependency of 4H-SiC is assumed to be similar because no experimental data is available.

The effective mass of electrons and holes has been measured by optically detected cyclotron resonance, or Raman scattering, and has been compared to theoretical calculation. Theoretical calculation reproduced well the experimental results.

There is no publication on measured data of bandgap narrowing. The theoretical calculation was first done by Lindefelt [13] and followed by Persson *et al.* [14]. The former model constitutes an extension of a semiempirical method originally developed by Jain and

Roulston [15]. The latter is based upon random phase approximation. Both calculations give the analytic form of band-edge displacement depending on the doping density. The analytic form corresponds to the `JainRoulston` model implemented in Sentaurus Device.

Figure 17 compares results from [13] and [14] with the Slotboom model implemented in Sentaurus Device with calibrated coefficients.

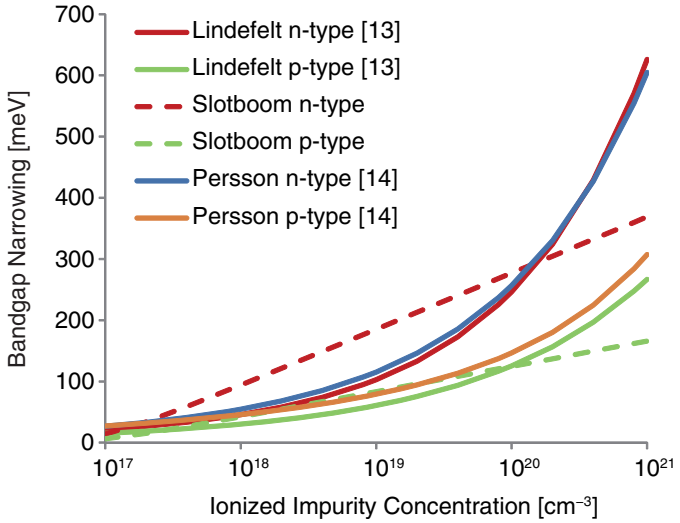

Figure 17 Bandgap narrowing of 4H-SiC [13][14]

Electron affinity is calculated assuming the linear dependency of hexagonality together with the measured band offset of the conduction band for 3C/6H and the calculated result of the band offset of the valence band.

Parameter sets for the Hatakeyama model [16] and the Okuto–Crowell impact ionization model are implemented in the parameter files (see Chapter 6 on page 39). The parameter set for the Okuto–Crowell impact ionization model along the c-axis corresponds to the one reported by Niwa *et al*. [17]. Comparison of the impact ionization coefficients of different references is shown in Figure 18 and Figure 19 on page 56.

Temperature dependency of thermal conductivity of 4H-SiC and 6H-SiC perpendicular to the c-axis has been reported in the literature. At low temperatures, T^3 dependency and T^2 dependency are observed for 4H-SiC and 6H-SiC, respectively. T^2 dependency is attributed to the scattering of phonons by electrons in the impurity band. Thermal conductivity in 6H-SiC single crystals decreases with increasing electron concentration, and the slope at low temperature can be represented by the T^2 law, which confirms the dominance of electron scattering. The temperature dependency of thermal conductivity using data of [18], [19], [20], and [21] as cited in [22] is implemented in the parameter files (see Chapter 6 on page 39). The experimental data is that in the direction perpendicular to the c-axis.

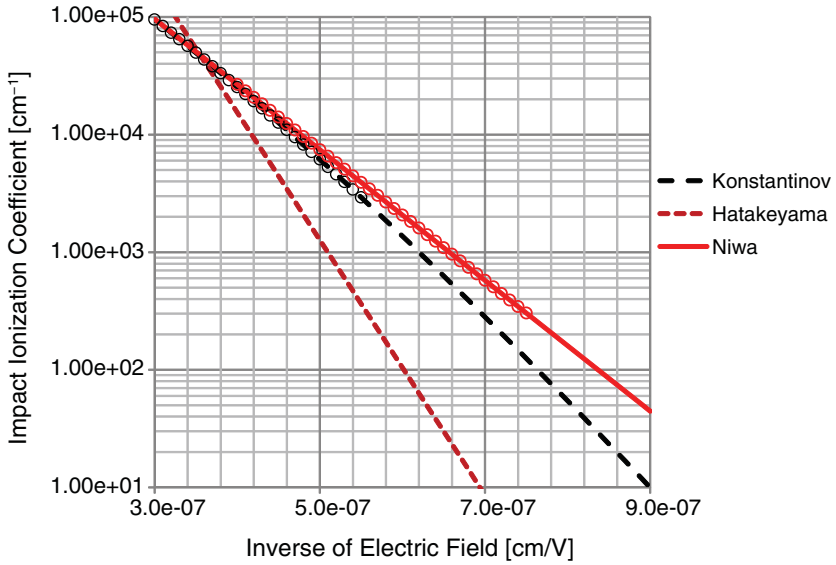

Figure 18 Hole impact ionization coefficient along c-axis of 4H-SiC [16][17][23]

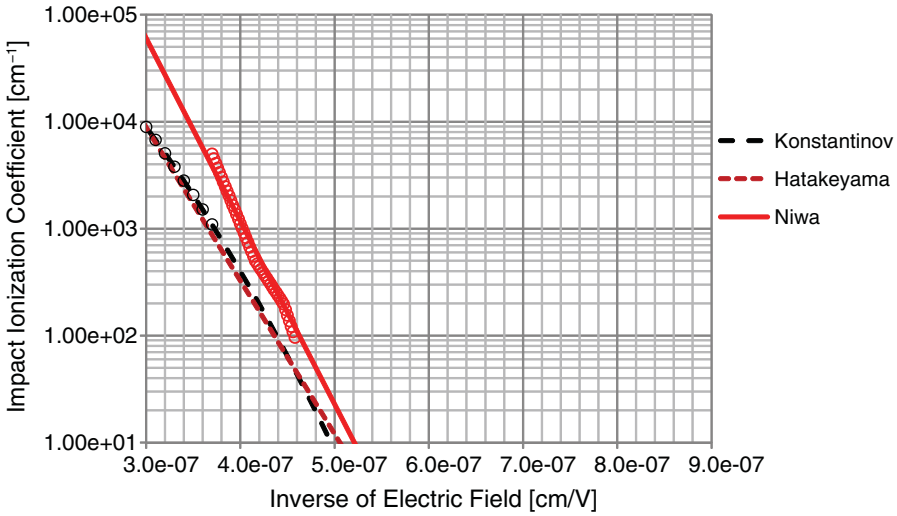

Figure 19 Electron impact ionization coefficient along c-axis of 4H-SiC [16][17][23]

Parameter sets for the Masetti and the Arora doping-dependent mobility models are implemented in the parameter files (see Chapter 6 on page 39). Figure 20 and Figure 21 show a comparison with different literature data.

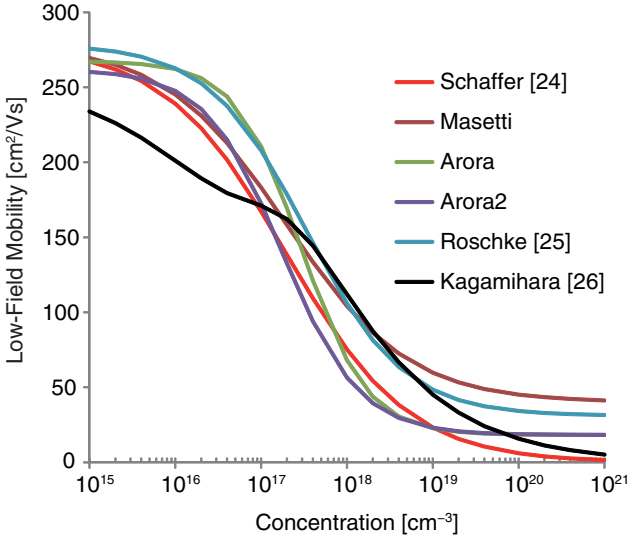

Figure 20 Doping-dependent electron mobility at 500 K for n-doped 4H-SiC [24][25][26]

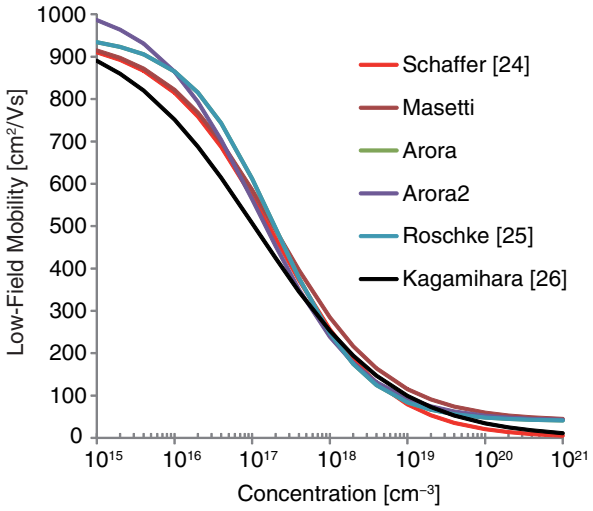

Figure 21 Doping-dependent electron mobility at 300 K for n-doped 4H-SiC [24][25][26]

For high-field saturation, all measured data refers to the current flow perpendicular to the c-axis. Parameters for the Canali model are extracted and implemented in the parameter file.

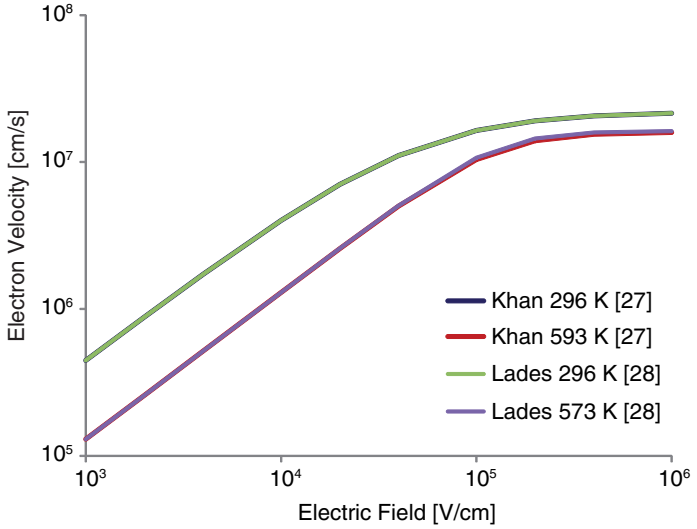

Figure 22 Drift velocity of electrons in 4H-SiC, parallel to basal plane (0001) [27][28]

A nitrogen atom residing on the C lattice site serves as the shallow donor in SiC. Phosphorus also is used as a shallow donor (like nitrogen) and has approximately the same ionization energy Ec-93 meV at the cubic site and Ec-53 meV at the hexagonal site. However, unlike nitrogen, P mainly substitutes at a silicon site, and less than 10% of substitutional P is at C sites. At C sites, P has a slightly larger ionization energy than that at the Si site. The ionization energy of N and P donors decreases with increasing donor concentration. Experimental data for cubic and hexagonal N donors in 6H-SiC is available. For N donors in 4H-SiC, experimental data of donor concentration dependency and fitting with empirically formula has been reported.

Aluminum and boron residing on Si lattice sites serve as the acceptors in SiC. For Al acceptors in 4H-SiC, experimental data of acceptor doping concentration dependency and fitting with empirical formulas have been reported in [29], [30], and [31].

Figure 23 on page 59 to Figure 27 on page 61 show the experimental data and the fit implemented in the parameter file.

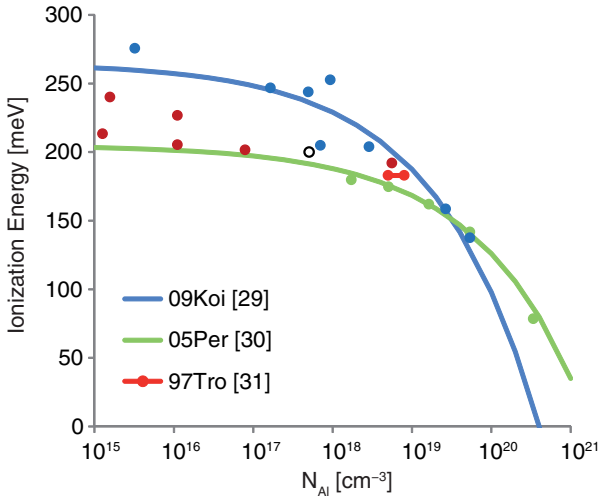

Figure 23 Ionization energy for aluminum-doped 4H-SiC together with extracted fit function [29][30][31]

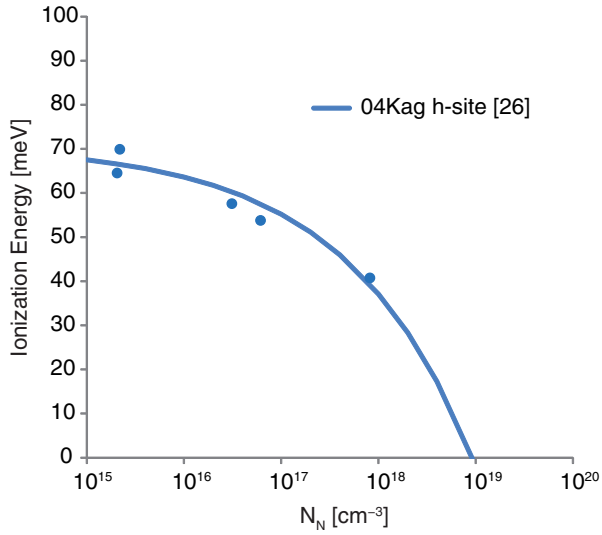

Figure 24 Ionization energy for nitrogen-doped 4H-SiC (hexagonal site) together with extracted fit function [26]

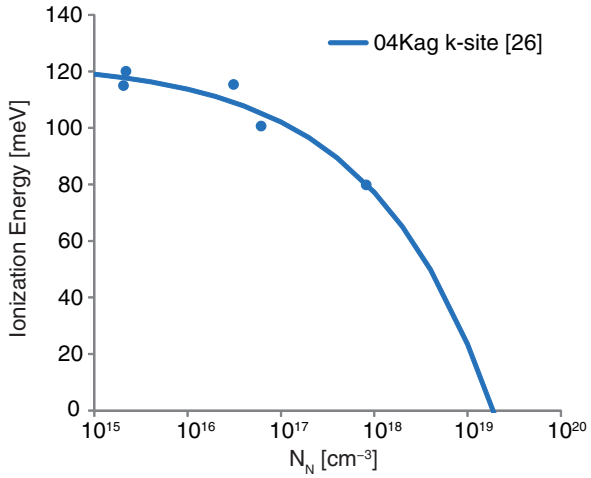

Figure 25 Ionization energy for nitrogen-doped 4H-SiC (cubic site) together with extracted fit function [26]

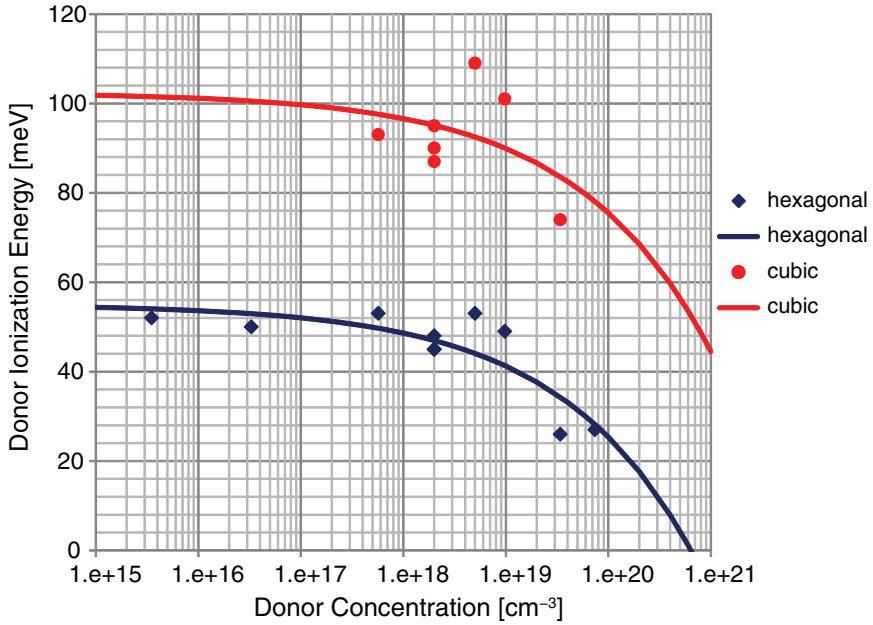

Figure 26 Ionization energy for phosphorus-doped 4H-SiC together with extracted fit function

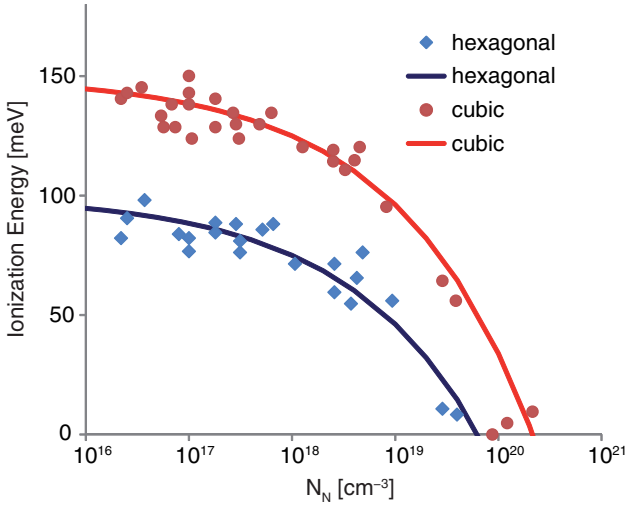

Figure 27 Ionization energy for nitrogen-doped 6H-SiC together with extracted fit function

Basic Properties of Indium Gallium Arsenide (InGaAs) Devices

The parameter values and the references can be found in the parameter file `InGaAs.par` in the `MaterialDB` folder of Sentaurus Device. The following sections briefly show the results of parameter calibration and review various aspects of the calibration.

Permittivity

The permittivity values for GaAs and InAs materials are reviewed following the data reported by Adachi [32]. Since there is no experimental data for semiconductor alloys, a linear interpolation scheme is adopted for $In_{1-x}Ga_xAs$ alloys.

Lattice Heat Capacity

Similarly, a linear interpolation scheme for heat capacity is used for $In_{1-x}Ga_xAs$ alloys, in which the heat capacity values for GaAs and InAs at 300 K are updated with the ones reported by Adachi [33].

Thermal Conductivity

The mole fraction dependency of thermal conductivity for $In_{1-x}Ga_xAs$ alloys has been measured by Abrahams *et al*. [34] and Arasly *et al*. [35] at 300 K. Due to a random distribution of Ga and In atoms in the sub-lattice sites, the thermal conductivity values for $In_{1-x}Ga_xAs$ alloys tend to be smaller than the corresponding binary materials. Figure 28 shows the thermal conductivity model and comparison to experimental data.

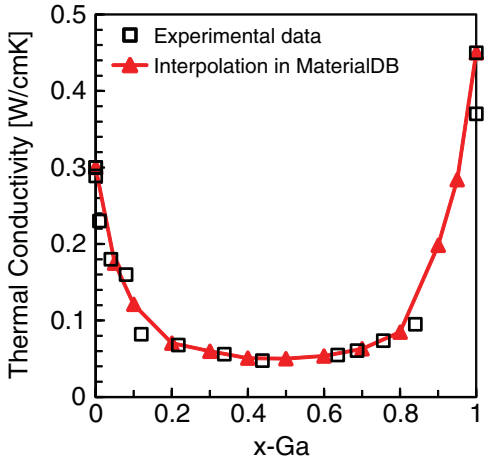

Figure 28 Thermal conductivity versus Ga mole fraction for $In_{1-x}Ga_xAs$ alloys at 300 K; experimental data taken from [34] and [35], and binary data taken from [36]

Band Gap and Electron Affinity

InGaAs ternary materials are direct bandgap materials over the entire composition range, and both the maxima of the upper valence bands and the minima of the conduction band are located at the Γ-point of the Brillouin zone. The photoluminescence and the photoreflectance measurements are often used to determine the bandgap energies of $In_{1-x}Ga_xAs$ [37][38][39]. In the case of the lattice-matched alloy to InP, $In_{0.53}Ga_{0.47}As$, which has been investigated extensively, the bandgap energy is generally recognized to be 0.816 eV at 0 K. Therefore, a temperature-independent bowing parameter of 0.477 eV is suggested [40]. As for the Varshni parameters, the values for $In_{1-x}Ga_xAs$ alloys are determined through a linear interpolation based on the ones from GaAs and InAs. In Figure 29 on page 63, the composition dependency of bandgap energy at 300 K has been plotted with the new set of bowing parameter and Varshni parameters. It is evident that the revised bandgap model fits well to the experimental data.

The electron affinity values for the GaAs and InAs binary materials are taken from Adachi [32] and are further derived to obtain the values at 0 K using the revised Varshni parameters. Since there is no much experimental data available, linearly interpolated electron affinity values are assumed for $In_{1-x}Ga_xAs$ alloys in the parameter file.

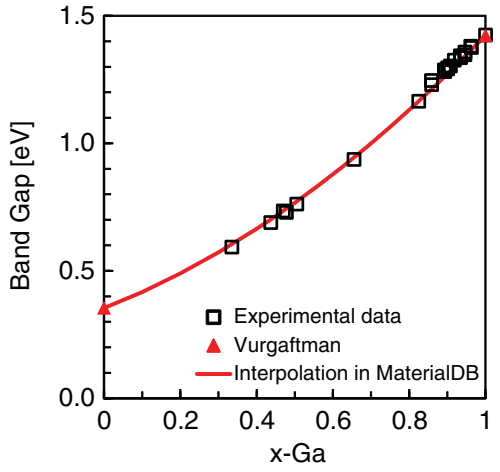

Figure 29 Band gap versus Ga mole fraction for $In_{1-x}Ga_xAs$ alloys at 300 K; experimental data is taken from [37], [38], [39]; and binary data is taken from [40]

Density-of-States

The electron effective masses for $In_{1-x}Ga_xAs$ alloys at the Γ-valley have been measured extensively [33], and the results are shown in Figure 30.

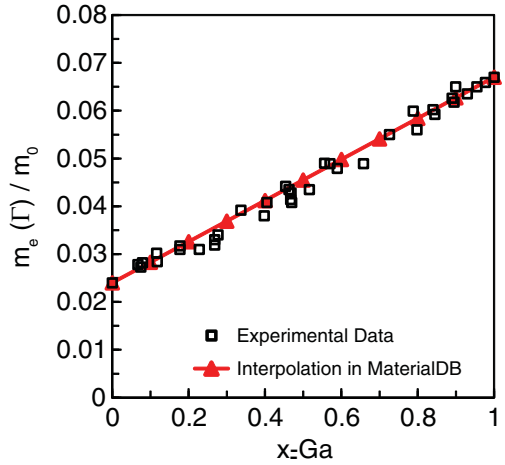

Figure 30 Electron effective mass at Γ-valley versus Ga mole fraction for $In_{1-x}Ga_xAs$ alloys at 300 K; experimental data is reprinted from Adachi [33]

A simple linear interpolation scheme using the corresponding GaAs and InAs binary data yields a good fit to the experimental data. In the $In_{1-x}Ga_xAs$ parameter file, the composition dependency of density-of-states for electrons is a set of tabulated values that are computed from the electron effective masses at 300 K using:

$$N_C(300\,\mathrm{K}) = 2.5094\times10^{19}\left(\frac{m_e}{m_0}\right)^{\frac{3}{2}} \tag{2}$$

Concerning the hole effective masses for $In_{1-x}Ga_xAs$ alloys, Vurgaftman *et al*. have proposed a bowing parameter for each Luttinger valence band parameter: γ_1, γ_2, γ_3 [40]. In measurement, $\kappa(x)$, defined as $\kappa = -1/3\gamma_1 + 2/3\gamma_2 + \gamma_3 - 2/3$, has been reported for $x = 0.47$ and $x = 0.82$–0.92 [41]–[43]. As shown in Figure 31, the interpolation scheme from Vurgaftman *et al*. agrees well to the experimental data to some extent and is then used for the calculation of composition dependency of the overall hole effective masses, m_p.

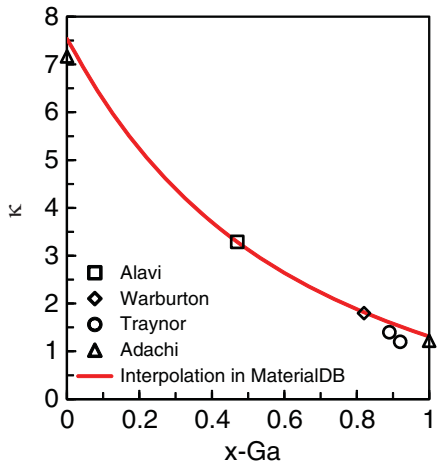

Figure 31 κ-values versus Ga mole fraction for $In_{1-x}Ga_xAs$ alloys; experimental data is taken from [32], [41], [42], and [43]; red line represents the interpolation function suggested by [40]

Similarly, a set of tabulated values of density-of-states for holes at 300 K is computed using:

$$N_V(300\,\mathrm{K}) = 2.5094\times10^{19}\left(\frac{m_p}{m_0}\right)^{\frac{3}{2}} \tag{3}$$

These tabulated values are included in Version N-2017.09 (see Figure 32 on page 65).

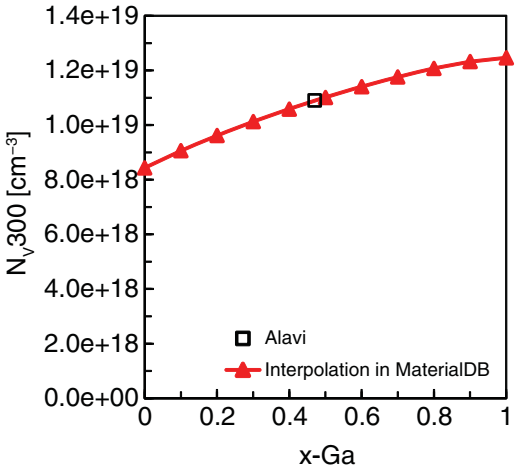

Figure 32 Valence band density-of-states at 300 K versus Ga mole fraction for $In_{1-x}Ga_xAs$ alloys; experimental data is computed based on Luttinger parameters taken from [41]; red line is computed following the interpolation scheme suggested by [40]

Bandgap Narrowing

Doping-dependent bandgap narrowing for GaAs, InAs, and $In_{1-x}Ga_xAs$ materials is accessed using the Jain–Roulston model [44]. The coefficients for p-type doping (A_p, B_p, C_p, and D_p) in GaAs material are derived from [44], in which the quantities are refined with available up-to-date basic material parameters of GaAs.

Figure 33 on page 66 shows the extent of bandgap narrowing for p-GaAs obtained with the Jain–Roulston model, and it agrees well with the experimental data measured using photoluminescence in the carrier density range of 2.7e17 to 3.9e20 cm^{-3} [45]–[49]. As for p-InAs, the coefficients are retrieved in the same way, but the model validation cannot be justified due to a lack of experimental data, as shown in Figure 34 on page 66.

Concerning n-type GaAs and InAs, the formulas in the Jain–Roulston model cannot describe the doping dependencies of bandgap narrowing. Then, the corresponding coefficients (A_n, B_n, C_n, and D_n) are determined preferably through curve fitting based on experimental data. As presented in Figure 33, the bandgap narrowing for n-GaAs with fitted Jain–Roulston coefficients agrees well with the experimental data [45][50]. It should be noted that, for n-InAs, the bandgap narrowing value reaches nearly 0.2 eV at the carrier density of 3e18 cm^{-3} [51], and a higher density is probable that would alter the band structure drastically. Therefore, a minimum bandgap (`EgMin`) value is set as 0.15 eV in the `Bandgap` model to avoid the occurrence of an abnormally low (or negative) band gap.

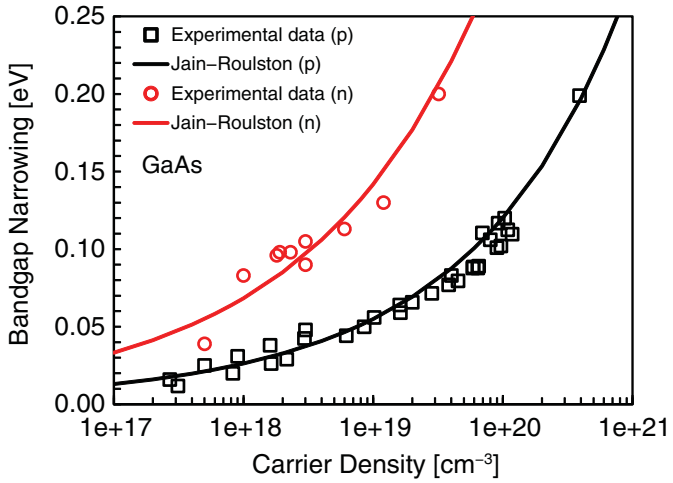

Figure 33 Doping-dependent bandgap narrowing for p-GaAs and n-GaAs at 300 K; experiment data is taken from [45]–[50]; black line is computed following Jain–Roulston model with up-to-date GaAs basic material parameters; red line is fitted curve based on experimental data from [45] and [50]

Since there is little experimental data reported in the literature to resolve the mole fraction dependency of bandgap narrowing for $In_{1-x}Ga_xAs$, a simple linear interpolation scheme is adopted for each coefficient in the Jain–Roulston model.

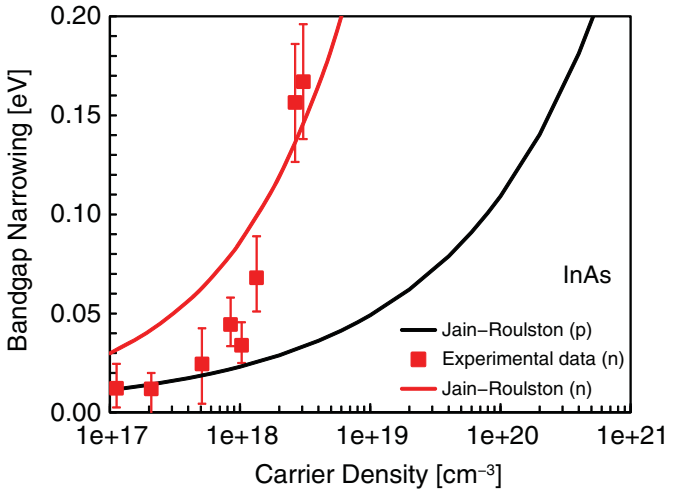

Figure 34 Doping-dependent bandgap narrowing for p-InAs and n-InAs at 300 K; black line is computed following Jain–Roulston model with up-to-date InAs basic material parameters; red line is fitted curve based on experimental data from [51]

Quantization Effects

The quantization model is considered in MOS devices to obtain the correct densities and field distributions in channels. The density gradient model in Sentaurus Device would be the first choice to be used for planar and nonplanar $In_{1-x}Ga_xAs$ device simulations, and then the calibration to the solutions from the Schrödinger equations is required to extract the corresponding quantization parameters.

The 1D Schrödinger solver in Sentaurus Band Structure provides a reference in terms of carrier density distribution in the inversion layer, and the fitting factor (γ) in the density gradient model then is fitted by minimizing the root-mean-square error of the charge integral over a range of applied gate voltages between these two approaches. The quantization parameter depends on the carrier polarity, the lattice orientation, the material composition, the layer thickness, the channel geometry, and the strain. In the `MaterialDB` folder, the fitted γ values in the `QuantumPotentialParameters` parameter set are provided for simulations in bulk configuration, as well as in double-gate simulations with channel thicknesses of 10 nm and 20 nm, for unstrained $In_{1-x}Ga_xAs$ alloys.

Note that, for $In_{1-x}Ga_xAs$ materials, the electron occupancy in other valleys (that is, L-valley) cannot be neglected at a relatively higher gate voltage. Therefore, the inclusion of the multivalley band structure model in the simulation allows users to determine the electron density-of-states more accurately.

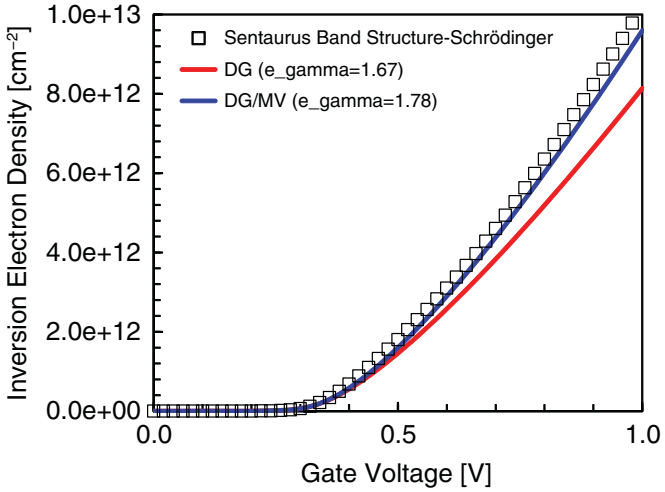

Figure 35 Inversion electron densities for a 10 nm thick double-gate (110) MOS structure with $In_{0.53}Ga_{0.47}As$ channel: red line is simulated with density gradient model and blue line is simulated with combination of multivalley and density gradient models; in both cases, e_gamma parameters have been optimized

The parameters for the `MultiValley` model in the `MaterialDB` folder of Version N-2017.09 with mole fraction dependency have been reviewed following some literature references [33][40] and the EPM band-structure calculation.

As shown in Figure 35 on page 67, the electron charge integral in a 10 nm thick $In_{0.53}Ga_{0.47}As$ double-gate structure simulated with the combination of the multivalley and density gradient models fits better to the result obtained with the Schrödinger solver of Sentaurus Band Structure, compared to the one with the density gradient model only. A similar conclusion can be drawn when observing the carrier distributions at a 1 V gate voltage along the 10 nm channel, as presented in Figure 36.

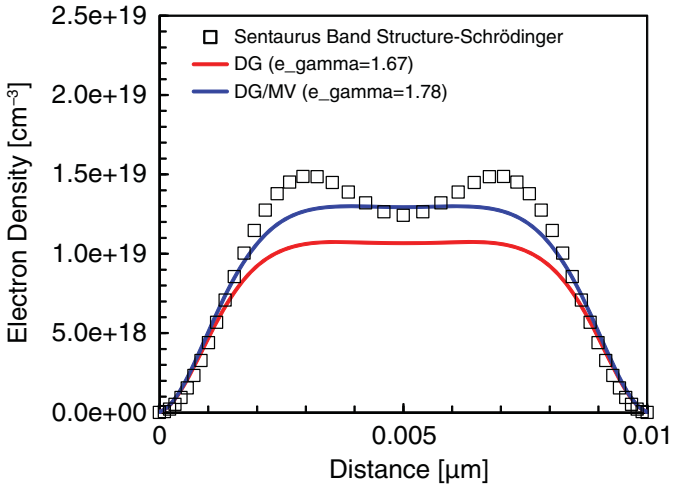

Figure 36 Carrier distributions at gate voltage of 1 V for a 10 nm thick double-gate (110) MOS structure with $In_{0.53}Ga_{0.47}As$ channel: red line is simulated with density gradient model and blue line is simulated with combination of multivalley and density gradient models; in both cases, e_gamma parameters have been optimized

Figure 37 on page 69 shows the tabulated values of fitted `e_gamma` and `h_gamma` parameters using the density gradient and the multivalley models, which are provided in the `MaterialDB` folder for bulk (100) and (110) orientations. It is evident that there is no orientation dependency for the electron quantization parameter, and the compositional variation is also less distinct compared to the hole quantization parameter. Moreover, the quantization parameter is also a function of layer thickness, as shown in Figure 38 on page 69.

It is important to implement the corresponding quantization parameters designated for a specific layer thickness during simulations, since the discrepancy on the charge distribution is very susceptible to thin layers. For example, the `e_gamma` value optimized for a 10 nm channel width could still be used for quantum correction on a 20 nm thick channel, but with a slightly larger error. However, the same value may be only appropriate to be used for thin layers down to 8 nm. If the layer thickness is less than 8 nm, a quantization calibration procedure will be performed again to extract the correct quantization parameter.

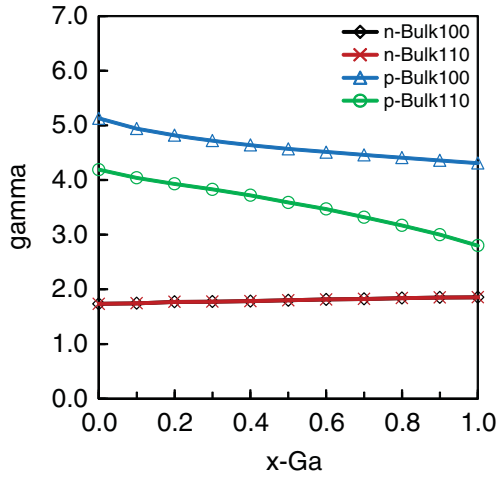

Figure 37 Fitted gamma values versus Ga mole fraction for bulk MOS structures with $In_{1-x}Ga_xAs$ alloys using density gradient and multivalley models

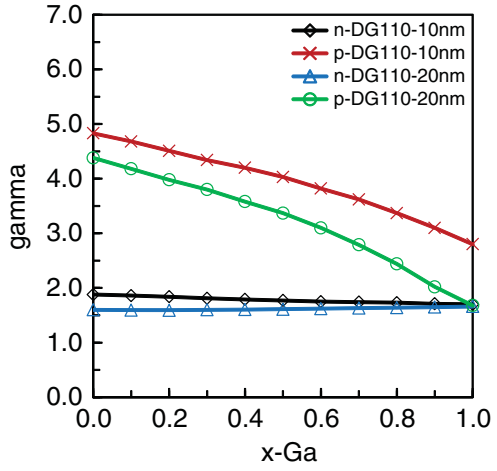

Figure 38 Fitted gamma values versus Ga mole fraction for 10 nm and 20 nm double-gate MOS structures with $In_{1-x}Ga_xAs$ alloys using density gradient and multivalley models

Low-Field Bulk Mobility and Its Doping Dependency

Low-field bulk mobility is a critical parameter to determine the current–voltage characteristics of InGaAs MIS devices and it is dependent on mole fraction, temperature, doping, inversion charge, and channel direction for unstrained InGaAs materials. Accurate theoretical models accounting for diverse scattering mechanisms can be complex and may be only applicable to

limited conditions. Therefore, empirical fitting based on available experimental data can serve as an alternative. In `MaterialDB` of Version N-2017.09, coefficients in the `ConstantMobility` and `DopingDependence` parameter sets of `InGaAs.par` have been reviewed and implemented following the empirical mobility model suggested in [52].

In [52], the fitting parameters in the empirical Caughey–Thomas mobility model for temperature and doping dependency are provided for unstrained GaAs, InAs, and $In_{0.53}Ga_{0.47}As$ materials. These parameters are transformed to the parameters of the Arora model for use in Sentaurus Device. Figure 39 demonstrates the doping dependency of electron mobility for unstrained GaAs and $In_{0.53}Ga_{0.47}As$ using the Arora model.

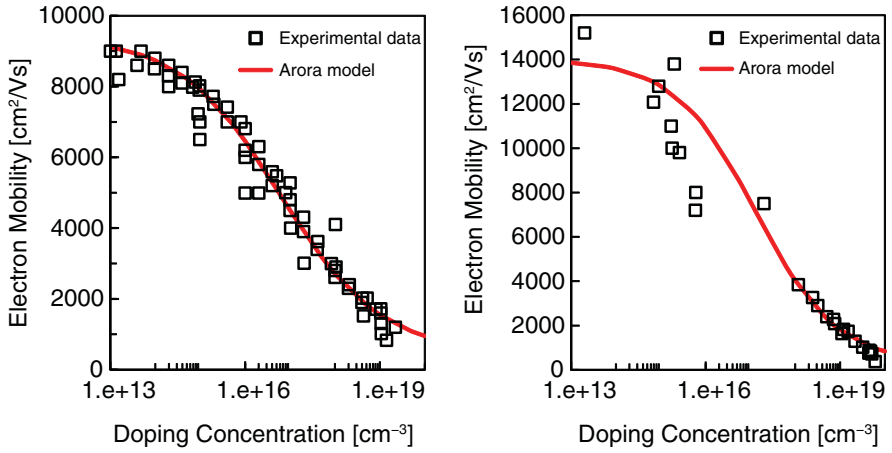

Figure 39 Doping-dependent low-field electron mobility for (*left*) GaAs and (*right*) $In_{0.53}Ga_{0.47}As$ at 300 K; red lines are computed following the Arora model with fitted parameters from [52]

The doping dependency of low-field mobility for $In_{1-x}Ga_xAs$ alloys, apart from $In_{0.53}Ga_{0.47}As$ material, is usually less investigated. Therefore, a two-sectional linear interpolation scheme is used based on InAs, $In_{0.53}Ga_{0.47}As$, and GaAs for each parameter in the Arora model. In Figure 40 on page 71, the compositional dependency of the low-field electron mobility for $In_{1-x}Ga_xAs$ alloys suggested in `MaterialDB` of Version N-2017.09 is shown together with some experimental data.

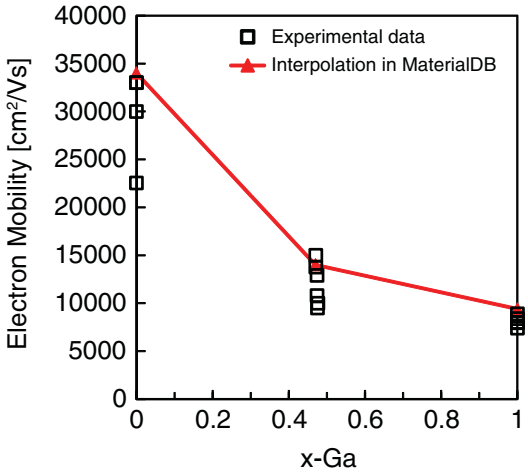

Figure 40 Low-field electron mobility at 300 K versus Ga mole fraction for $In_{1-x}Ga_xAs$ alloys; experimental data is reprinted from [53]; red line is the interpolation curve suggested in MaterialDB

Philips Unified Mobility Model

The Philips unified mobility model describes both majority and minority carrier mobility in bulk, taking into account phonon scattering, impurity scattering, carrier–carrier scattering, and screening of scattering processes. In the `MaterialDB` folder, the parameters for majority carrier mobility in InAs, $In_{0.53}Ga_{0.47}As$, and GaAs materials have been calibrated without considering the minority impurity scattering where other coefficients, such as the clustering functions and the screening parameters, are preserved as the default ones from silicon material.

The maximum carrier mobility (μ_{max}), the minimum carrier mobility (μ_{min}), and the exponent (θ) for $In_{1-x}Ga_xAs$ alloys are transformed from the corresponding `ConstantMobility` and Arora models. Then, the reference density (N_{ref}) and the exponent (α) coefficients can be fitted to the doping-dependent mobility given by the Arora model within a doping range between 1.0e13 cm^{-3} and 1.0e20 cm^{-3} for GaAs and $In_{0.53}Ga_{0.47}As$. Since the intrinsic density of InAs is relatively larger compared to GaAs and $In_{0.53}Ga_{0.47}As$, the fitting range for InAs is limited to the range 1e15 cm^{-3} to 1e20 cm^{-3}.

Figure 41 on page 72 presents the electron and hole mobility in $In_{0.53}Ga_{0.47}As$ material at various doping levels for the Philips unified mobility model with fitted coefficients.

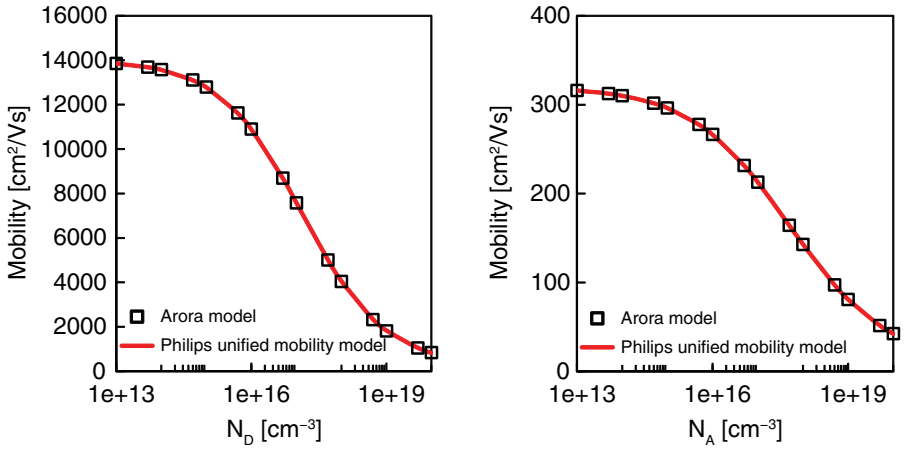

Figure 41 Doping-dependent low field mobility for (*left*) electron and (*right*) hole majority carriers in $In_{0.53}Ga_{0.47}As$ alloy at 300 K; red lines are computed with the Philips unified mobility model with fitted parameters suggested in MaterialDB

Inversion Layer Mobility

Inversion and Accumulation Layer Mobility Model

In a MOSFET device, the surface roughness and the surface phonon scattering can degrade carrier mobility at the proximity of a semiconductor–insulator interface due to a high electric field, normal to the channel interface imposed across the channel region. Since $In_{1-x}Ga_xAs$ alloys have the potential to realize n-MOSFET devices, parameter calibration with respect to available experimental data is required to establish a more accurate mobility degradation model.

This section briefly describes how the parameters in the `MaterialDB` folder were calibrated for the inversion and accumulation layer mobility (`IALMob`) model.

The calibration methodology involves two main sequences and concerns primarily the electron mobility in the inversion layer. First, with some initial calibrations with respect to the experimental data to account for the process variations, the 1D mobility calculator in Sentaurus Band Structure provides a reference in terms of mobility in the inversion layer for the entire mole fraction range. The experimental data used for this step of the mobility calibration was reported by Xuan *et al*. [54] on an inversion-type n-channel $In_{0.53}Ga_{0.47}As$ MOSFET with 8 nm thick ALD Al_2O_3 as the gate dielectric. Later, the coefficients of each scattering mechanism of the `IALMob` model are extracted by comparing the mobility values between these two simulation approaches.

As shown in Figure 42, the dispersion curves of the mobility field in the $In_{0.53}Ga_{0.47}As$ inversion layer have been simulated using the Sentaurus Band Structure mobility calculator with diverse combinations of scattering models, in which the parameters Δ and Λ of the surface-roughness power-spectrum model with exponential density function have been optimized for effective electric field in the range of 0.6–1.0 MV/cm. Afterwards, the mobility offset with respect to experimental data, after considering all the available scattering models such as alloy, surface roughness, phonon, and Coulomb scattering, as well as the fixed charge trap model, can be reduced further in the range of 0.1–0.4 MV/cm by adjusting the interface charge density.

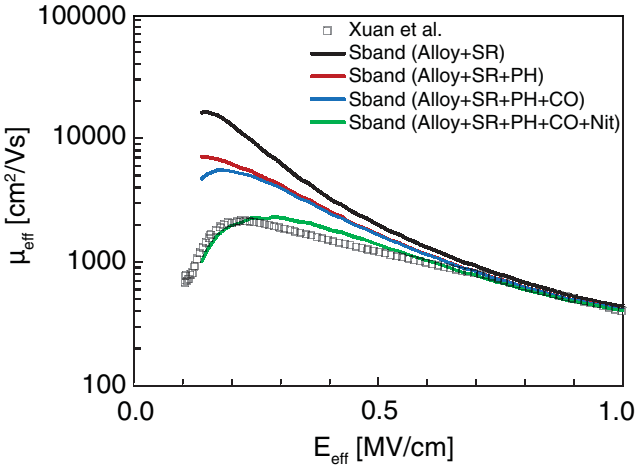

Figure 42 Effective electron mobility versus effective electric field for $In_{0.53}Ga_{0.47}As$ (p-doping=1e17 cm^{-3} in channel) MOSFET with ALD Al_2O_3; simulation results are obtained using 1D mobility calculator of Sentaurus Band Structure with various combinations of alloy, surface roughness (SR), phonon (PH), and Coulomb (CO) scattering models, in which the surface roughness parameters (Δ=2.2e-7 cm; Λ=4.6e-8 cm) and the interface charge density (N_{it}=4.3e12 cm^{-2}) have been calibrated; experimental data is taken from [54]

As for the `IALMob` model, the calibration was performed with the parameters of 3D phonon scattering and 3D Coulomb scattering taken from the constant mobility model and the Philips unified mobility model, respectively, and the 2D and 3D parts of phonon scattering are combined with `PhononCombination=1`. Since it is necessary to distinguish the contribution of various scattering mechanisms in the `IALMob` model, first 2D Coulomb scattering is disregarded by designating a large value in factors such as $D_{1,inv}$ and $D_{2,inv}$. Then, the resulting effective mobility values are compared to Sentaurus Band Structure results, for which only surface roughness scattering and phonon scattering are enabled, for p-doping ranging between 1e15 and 1e18 cm^{-3}.

At this step, the reviewed parameters principally include coefficients accounting for 2D phonon scattering (`B`, `C`, and λ) and those representing surface roughness scattering (δ, `A*`, and λ_{sr}), where the λ and λ_{sr} coefficients describe the doping dependencies of phonon and

surface roughness scattering, respectively. Other parameters are kept as the ones for silicon material.

After the coefficients for surface roughness scattering and 2D phonon scattering are determined, the parameters for 2D Coulomb scattering ($D_{1,inv}$, $D_{2,inv}$, and $\nu_{1,inv}$) can be fitted with respect to Sentaurus Band Structure results when Coulomb scattering is implemented.

Figure 43 compares the effective electron mobility versus sheet density at various p-doping levels in the channel region between the `IALMob` model with calibrated parameters and Sentaurus Band Structure results for $In_{0.53}Ga_{0.47}As$, InAs, and GaAs. Regarding the interpolation scheme for the `IALMob` model in $In_{1-x}Ga_xAs$ alloys, a two-sectional linear curve is used, based on $In_{0.53}Ga_{0.47}As$, InAs, and GaAs for each parameter previously mentioned.

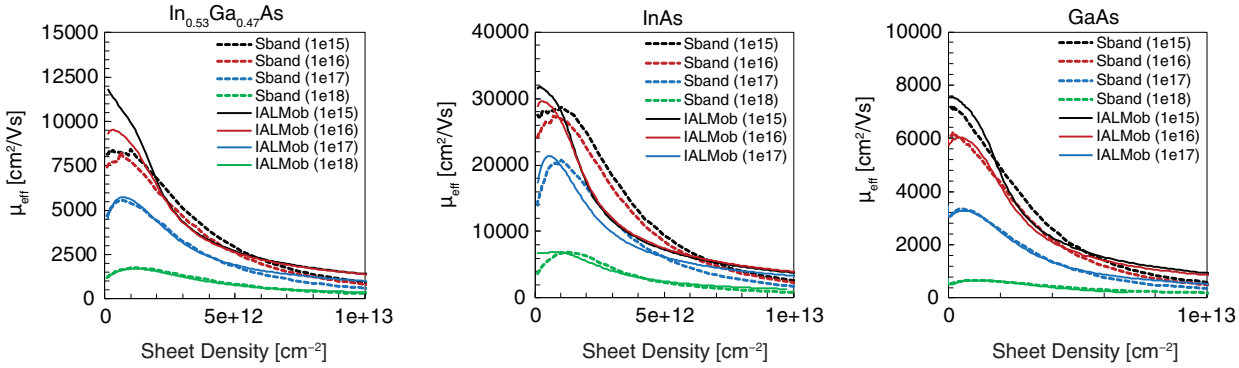

Figure 43 Effective electron mobility versus sheet density (*left*) $In_{0.53}Ga_{0.47}As$, (*middle*) InAs, and (*right*) GaAs MOSFET with ALD Al_2O_3 at various p-doping levels in the channel region; dotted lines are obtained using 1D mobility calculator of Sentaurus Band Structure with combination of surface roughness (SR), phonon (PH), and Coulomb (CO) scattering models, and the alloy scattering model is further considered for $In_{0.53}Ga_{0.47}As$; thick lines are obtained using IALMob model with calibrated parameters suggested in MaterialDB

Interface Charge Mobility Model

Following the results of mobility calibration for the `IALMob` model, the mobility degradation model due to the interface charges was reviewed further, including the `NegInterfaceCharge` and `PosInterfaceCharge` components in Sentaurus Device. As shown in Figure 42 on page 73, the Sentaurus Band Structure mobility calculator can fit well to the experimental data from Xuan *et al.* [54] when interface charge density (N_{it}) is fitted to be 4.3e12 cm^{-2}.

To calibrate parameters such as μ_1, C_{trans}, l_{crit}, and E_0 for the `NegInterfaceCharge` and `PosInterfaceCharge` models, the mobility values for two more N_{it} levels, 0 and 2.0e12, are also computed using Sentaurus Band Structure. Figure 44 on page 75 presents the curves of mobility versus field for $In_{0.53}Ga_{0.47}As$ material when implementing the `IALMob` model and the

negative and positive interface charge density models with calibrated parameters with respect to Sentaurus Band Structure results. Similar to other mobility models, the interpolation scheme for the `NegInterfaceCharge` and `PosInterfaceCharge` models in $In_{1-x}Ga_xAs$ alloys also uses a two-sectional linear curve based on InAs, $In_{0.53}Ga_{0.47}As$, and GaAs.

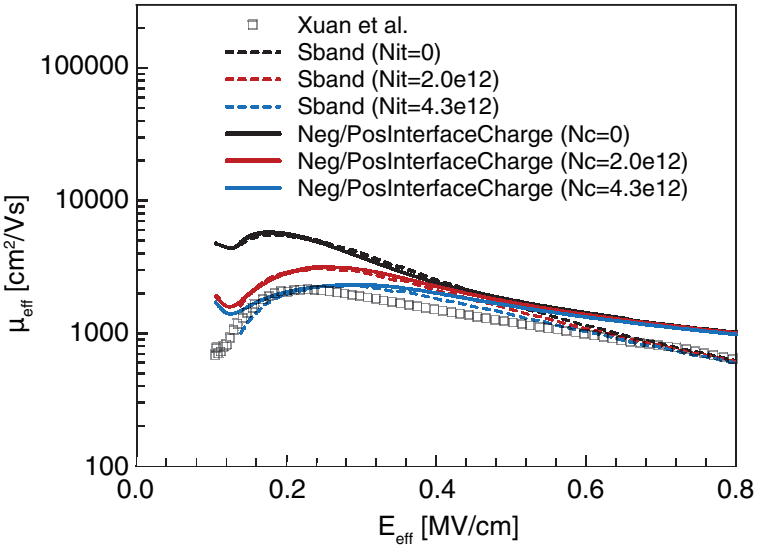

Figure 44 Effective electron mobility versus effective electric field for $In_{0.53}Ga_{0.47}As$ (p-doping=1e17 cm^{-3} in channel) MOSFET with ALD Al_2O_3; dotted lines are obtained using 1D mobility calculator of Sentaurus Band Structure with combination of alloy, surface roughness (SR), phonon (PH), and Coulomb (CO) scattering models, as well as interface trap model with charge density of 0, 2.0e12, and 4.3e12 cm^{-2}; thick lines are obtained using NegInterfaceCharge and PosInterfaceCharge models with calibrated parameters suggested in MaterialDB

Strained Low-Field Mobility

Multivalley Subband Electron Mobility Model

Mechanical stress in devices leads to a change in band structure and carrier mobility, and is considered an approach to enhance mobility. The multivalley electron mobility (`eSubband`) model with default parameters has been tested on several $In_{1-x}Ga_xAs$-based FETs on which either uniaxial or biaxial stress is applied [55][56][57][58]. The simulations reproduce the trend of electron mobility enhancement for tensile stress. However, the enhancement generally tends to be lower than for experimental data.

Since the investigated device structures and conditions are still very diverse and incomplete, a more unified and better set of model parameters has not been established (for example, to

consider the dependencies on mole fraction and geometry for $In_{1-x}Ga_xAs$ materials) and default parameters have been kept.

Piezoresistive Mobility Model

Due to a lack of experimental results reported in the literature for $In_{1-x}Ga_xAs$ alloys, the related piezoresistive coefficients are difficult to determine. Nainani *et al*. [59] have demonstrated the conductivity extraction for n-$In_{0.2}Ga_{0.8}As$ material using the transfer length method and suggest a similar value for the longitudinal piezoresistive coefficient for n-$In_{0.2}Ga_{0.8}As$ as for n-Si.

Basic Properties of Silicon Germanium (SiGe) Devices

Parameters for SiGe MOS devices are contained in the `SiliconGermaniumc100.par` and `SiliconGermaniumc110.par` parameter files in the `MaterialDB` folder of Sentaurus Device. The complete content of these files is described in Chapter 6 on page 39.

Permittivity

The low-frequency relative dielectric constant values are interpolated linearly between the corner values of 11.7 (silicon) and 16.2 (germanium) for each Ge mole fraction (see [60]).

Thermal Conductivity

The mole fraction dependency of the thermal conductivity is extracted from data from Schaffler [60] (see Figure 45). Data is implemented piecewise linearly in the parameter file.

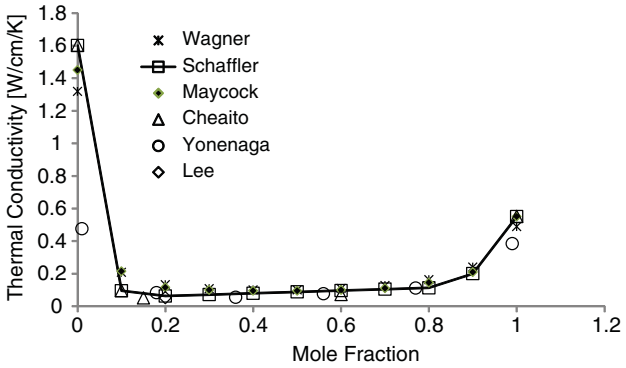

Figure 45 Thermal conductivity versus mole fraction ([60][61][62][63][64][65]; solid line implementation in MaterialDB parameter file)

Band Structure

Band structure data (band gap and affinity) is extracted from [66] (see Figure 46 and Figure 47 on page 78). The bandgap narrowing is extracted from Jain and Roulston [15] (see Figure 48 on page 78) where the `OldSlotboom` model is used for fitting (refer to the *Sentaurus™ Device User Guide*). Linear interpolation between silicon and germanium values is performed for the prefactor of the `OldSlotboom` model to describe the mole fraction dependency. All data is implemented piecewise linearly in the parameter file.

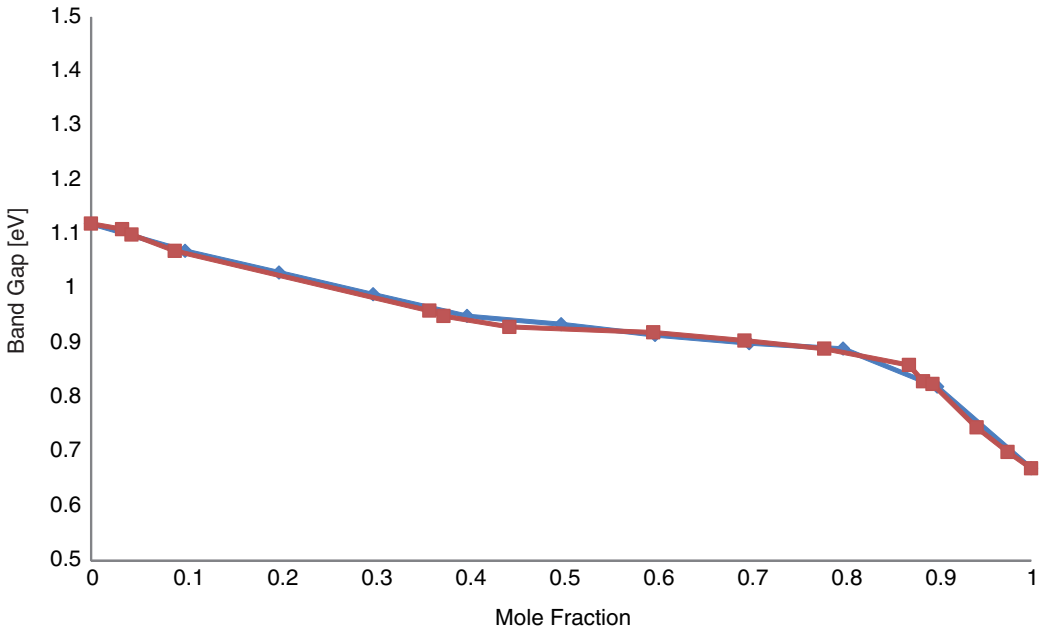

Figure 46 Band gap as a function of mole fraction

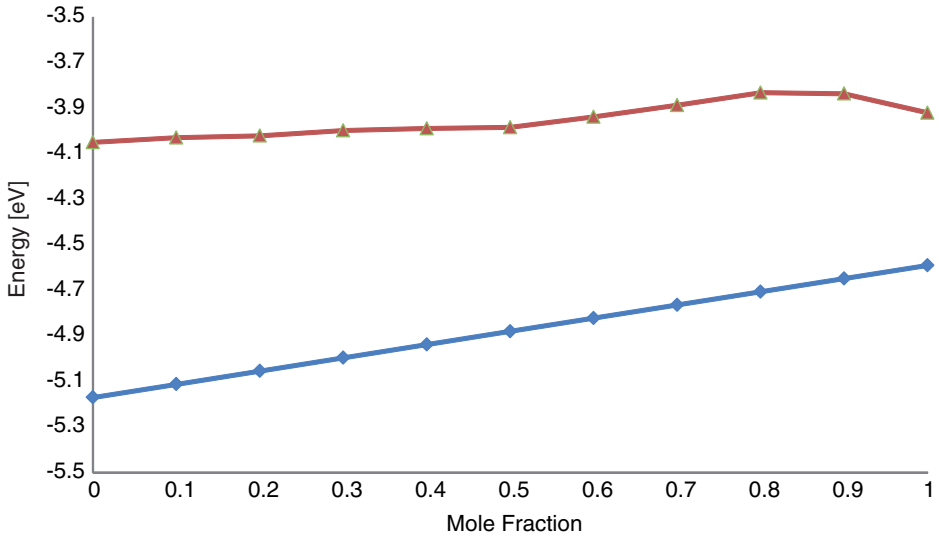

Figure 47 Conduction and valence bands as a function of mole fraction

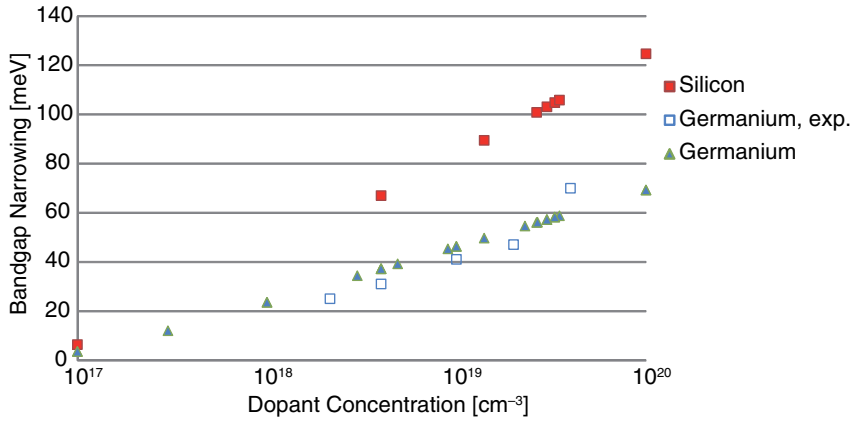

Figure 48 Bandgap narrowing for silicon and germanium (for this figure, a prefactor of the OldSlotboom model of 5 meV is used)

Bulk Low-Field Mobility

The bulk low-field mobility `PhuMob` model parameters for silicon, SiGe, and germanium are extracted from different measurements with the focus on the data from Golikova *et al*. [67] and Fistul' *et al*. [68]. The results of this calibration are shown in Figure 49 for germanium. The model parameters are implemented piecewise linearly.

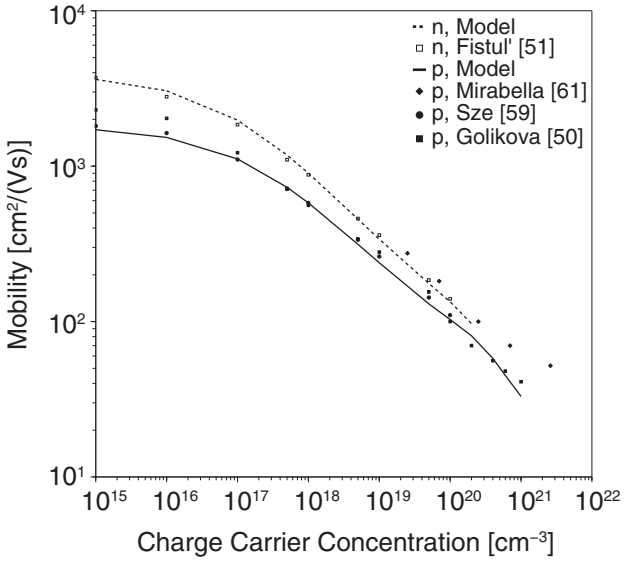

Figure 49 Measurements from different sources ([67][68][69][70][71]) for the doping dependency of the electron and hole mobility in Ge and the implementation in the Sentaurus Device parameter files (lines)

References

[1] S. Takagi *et al*., "On the Universality of Inversion Layer Mobility in Si MOSFET's: Part I—Effects of Substrate Impurity Concentration," *IEEE Transactions on Electron Devices*, vol. 41, no. 12, pp. 2357–2362, 1994.

[2] S. Takagi *et al*., "On the Universality of Inversion Layer Mobility in Si MOSFET's: Part II—Effects of Surface Orientation," *IEEE Transactions on Electron Devices*, vol. 41, no. 12, pp. 2363–2368, 1994.

[3] H. Nakamura *et al*., "Effects of Selecting Channel Direction in Improving Performance of Sub-100 nm MOSFETs Fabricated on (110) Surface Si Substrate," *Japanese Journal of Applied Physics*, vol. 43, no. 4B, pp. 1723–1728, 2004.

[4] H. M. Nayfeh *et al*., "Influence of High Channel Doping on the Inversion Layer Electron Mobility in Strained Silicon n-MOSFETs," *IEEE Electron Device Letters*, vol. 24, no. 4, pp. 248–250, 2003.

[5] C. D. Young *et al*., "(110) and (100) Sidewall-oriented FinFETs: A performance and reliability investigation," *Solid-State Electronics*, vol. 78, pp. 2–10, December 2012.

[6] A. T. Pham, C. Jungemann, and B. Meinerzhagen, "Modeling and validation of piezoresistive coefficients in Si hole inversion layers," *Solid-State Electronics*, vol. 53, no. 12, pp. 1325–1333, 2009.

[7] F. M. Bufler, A. Erlebach, and M. Oulmane, "Hole Mobility Model With Silicon Inversion Layer Symmetry and Stress-Dependent Piezoconductance Coefficients," *IEEE Electron Device Letters*, vol. 30, no. 9, pp. 996–998, 2009.

[8] P. Packan *et al*., "High Performance Hi-K + Metal Gate Strain Enhanced Transistors on (110) Silicon," in *IEDM Technical Digest*, San Francisco, CA, USA, December 2008.

[9] R. Chau *et al*., "High-κ/Metal–Gate Stack and Its MOSFET Characteristics," *IEEE Electron Device Letters*, vol. 25, no. 6, pp. 408–410, 2004.

[10] M. Cassé *et al*., "Carrier Transport in HfO_2/Metal Gate MOSFETs: Physical Insight Into Critical Parameters," *IEEE Transactions on Electron Devices*, vol. 53, no. 4, pp. 759–768, 2006.

[11] N. Stavitski *et al*., "Evaluation of Transmission Line Model Structures for Silicide-to-Silicon Specific Contact Resistance Extraction," *IEEE Transactions on Electron Devices*, vol. 55, no. 5, pp. 1170–1176, 2008.

[12] Y. Asahi, *Physical parameters for 4H-SiC and 6H-SiC*, Internal Report, Mountain View, California: Synopsys, Inc., November 2012.

[13] U. Lindefelt, "Doping-induced band edge displacements and band gap narrowing in 3C–, 4H–, 6H–SiC, and Si," *Journal of Applied Physics*, vol. 84, no. 5, pp. 2628–2637, 1998.

[14] C. Persson, U. Lindefelt, and B. E. Sernelius, "Bang gap narrowing in n-type and p-type 3C–, 2H–, 4H–, 6H–SiC, and Si," *Journal of Applied Physics*, vol. 86, no. 8, pp. 4419–4427, 1999.

[15] S. C. Jain and D. J. Roulston, "A Simple Expression for Band Gap Narrowing (BGN) in Heavily Doped Si, Ge, GaAs and Ge_xSi_{1-x} Strained Layers," *Solid-State Electronics*, vol. 34, no. 5, pp. 453–465, 1991.

[16] T. Hatakeyama *et al*., "Impact ionization coefficients of 4H silicon carbide," *Applied Physics Letters*, vol. 85, no. 8, pp. 1380–1382, 2004.

[17] H. Niwa, J. Suda, and T. Kimoto, "Temperature Dependence of Impact Ionization Coefficients in 4H-SiC," *Materials Science Forum*, vol. 778-780, pp. 461–466, 2014.

[18] Y. S. Touloukian and E. H. Buyco, *Specific Heat–Nonmetallic Solids*, Thermophysical Properties of Matter, TPRC Data Series, vol. 5, IFI/Plenum: New York, 1970.

[19] Y. S. Touloukian and C. Y. Ho (eds.), *Thermal Conductivity–Nonmetallic Solids*, Thermophysical Properties of Matter, TPRC Data Series, vol. 2, IFI/Plenum: New York, 1970.

[20] E. A. Burgemeister, W. von Muench, and E. Pettenpaul, "Thermal conductivity and electrical properties of 6*H* silicon carbide," *Journal of Applied Physics*, vol. 50, no. 9, pp. 5790–5794, 1979.

[21] D. Morelli *et al.*, "Carrier concentration dependence of the thermal conductivity of silicon carbide," in *5th Silicon Carbide and Related Materials Conference*, Washington, DC, USA, pp. 313–315, November 1993.

[22] D. T. Morelli *et al.*, "Phonon-electron scattering in single crystal silicon carbide," *Applied Physics Letters*, vol. 63, no. 23, pp. 3143–3145, 1993.

[23] A. O. Konstantinov *et al.*, "Ionization rates and critical fields in 4H silicon carbide," *Applied Physics Letters*, vol. 71, no. 1, pp. 90–92, 1997.

[24] W. J. Schaffer *et al.*, "Conductivity Anisotropy in Epitaxial 6H and 4H SiC," in *MRS Symposium Proceedings, Diamond, SiC and Nitride Wide Bandgap Semiconductors*, vol. 339, San Francisco, CA, USA, pp. 595–600, April 1994.

[25] M. Roschke and F. Schwierz, "Electron Mobility Models for 4H, 6H, and 3C SiC," *IEEE Transactions on Electron Devices*, vol. 48, no. 7, pp. 1442–1447, 2001.

[26] S. Kagamihara *et al.*, "Parameters required to simulate electric characteristics of SiC devices for *n*-type 4H–SiC," *Journal of Applied Physics*, vol. 96, no. 10, pp. 5601–5606, 2004.

[27] I. A. Khan and J. A. Cooper, Jr., "Measurement of High Field Electron Transport in Silicon Carbide," *Materials Science Forum*, vol. 264-268, pp. 509–512, February 1998.

[28] M. Lades, *Modeling and Simulation of Wide Bandgap Semiconductor Devices: 4H/6H-SiC*, Ph.D. thesis, Technischen Universität, Munich, Germany, 2000.

[29] A. Koizumi, J. Suda, and T. Kimoto, "Temperature and doping dependencies of electrical properties in Al-doped 4*H*-SiC epitaxial layers," *Journal of Applied Physics*, vol. 106, no. 1, p. 013716, 2009.

[30] J. Pernot, S. Contreras and J. Camassel, "Electrical transport properties of aluminum-implanted 4H–SiC," *Journal of Applied Physics*, vol. 98, no. 2, p. 023706, 2005.

[31] T. Troffer *et al.*, "Doping of SiC by Implantation of Boron and Aluminum," *Physica Status Solidi (a)*, vol. 162, no. 1, pp. 277–298, 1997.

[32] S. Adachi, *Properties of Group-IV, III–V and II–VI Semiconductors*, West Sussex, England: John Wiley & Sons, 2005.

[33] S. Adachi, *Properties of Semiconductor Alloys: Group-IV, III–V and II–VI Semiconductors*, West Sussex, England: John Wiley & Sons, 2009.

[34] M. S. Abrahams, R. Braunstein, and F. D. Rosi, "Thermal, Electrical and Optical Properties of (In,Ga)As Alloys," *Journal of Physics and Chemistry of Solids*, vol. 10, no. 2–3, pp. 204–210, 1959.

[35] D. G. Arasly, R. N. Ragimov, and M. I. Aliev, "Characteristics of phonon scattering in $Ga_xIn_{1-x}As$ solid solutions," *Soviet Physics Semiconductors*, vol. 24, no. 2, pp. 225–226, 1990.

[36] S. Adachi, "Lattice thermal conductivity of group-IV and III-V semiconductor alloys," *Journal of Applied Physics*, vol. 102, p. 063502, September 2007.

[37] R. E. Nahory, M. A. Pollack, and J. C. DeWinter, "Growth and characterization of liquid-phase epitaxial $In_xGa_{1-x}As$," *Journal of Applied Physics*, vol. 46, no. 2, pp. 775–782, 1975.

[38] T. J. Kim *et al.*, "Dielectric functions of $In_xGa_{1-x}As$ alloys," *Physical Review B*, vol. 68, no. 11, p. 115323, 2003.

[39] D. K. Gaskill *et al.*, "Band-gap determination by photoreflectance of InGaAs and InAlAs lattice matched to InP," *Applied Physics Letters*, vol. 56, no. 13, pp. 1269–1271, 1990.

[40] I. Vurgaftman, J. R. Meyer, and L. R. Ram-Mohan, "Band parameters for III–V compound semiconductors and their alloys," *Journal of Applied Physics*, vol. 89, no. 11, pp. 5815–5875, 2001.

[41] K. Alavi, R. L. Aggarwal, and S. H. Groves, "Interband magnetoabsorption of $In_{0.53}Ga_{0.47}As$," *Physical Review B*, vol. 21, no. 3, pp. 1311–1315, 1980.

[42] R. J. Warburton *et al.*, "Valence band spin splitting in strained $In_{0.18}Ga_{0.82}As$/GaAs quantum wells," *Semiconductor Science and Technology*, vol. 6, no. 5, pp. 359–364, 1991.

[43] N. J. Traynor *et al.*, "Highly nonlinear Zeeman splitting of excitons in semiconductor quantum wells," *Physical Review B*, vol. 55, no. 23, pp. 15701–15705, 1997.

[44] S. C. Jain, J. M. McGregor, and D. J. Roulston, "Band-gap narrowing in novel III-V semiconductors," *Journal of Applied Physics*, vol. 68, no. 7, pp. 3747–3749, 1990.

[45] G. Borghs *et al.*, "Band-gap narrowing in highly doped *n*- and *p*-type GaAs studied by photoluminescence spectroscopy," *Journal of Applied Physics*, vol. 66, no. 9, pp. 4381–4386, 1989.

[46] B. J. Aitchison *et al.*, "Enhanced hot-electron photoluminescence from heavily carbon-doped GaAs," *Applied Physics Letters*, vol. 56, no. 12, pp. 1154–1156, 1990.

[47] D. Olego and M. Cardona, "Photoluminescence in heavily doped GaAs. I. Temperature and hole-concentration dependence," *Physical Review B*, vol. 22, no. 2, pp. 886–893, 1980.

[48] Z. H. Lu, M. C. Hanna, and A. Majerfeld, "Determination of band gap narrowing and hole density for heavily C-doped GaAs by photoluminescence spectroscopy," *Applied Physics Letters*, vol. 64, no. 1, pp. 88–90, 1994.

[49] B. P. Yan, J. S. Luo, and Q. L. Zhang, "Study of band-gap narrowing effect and nonradiative recombination centers for heavily C-doped GaAs by photoluminescence spectroscopy," *Journal of Applied Physics*, vol. 77, no. 9, pp. 4822–4824, 1995.

[50] H. Yao and A. Compaan, "Plasmons, photoluminescence, and band-gap narrowing in very heavily doped *n*-GaAs," *Applied Physics Letters*, vol. 57, no. 2, pp. 147–149, 1990.

[51] N. A. Semikolenova, I. M. Nesmelova, and E. N. Khabarov, "Investigation of the impurity interaction mechanism in indium arsenide," *Soviet Physics Semiconductors*, vol. 12, no. 10, pp. 1139–1142, 1978.

[52] M. Sotoodeh, A. H. Khalid, A. A. Rezazadeh, "Empirical low-field mobility model for III–V compounds applicable in device simulation codes," *Journal of Applied Physics*, vol. 87, no. 6, pp. 2890–2900, 2000.

[53] Ch. Köpf, H. Kosina, and S. Selberherr, "Physical Models for Strained and Relaxed GaInAs Alloys: Band Structure and Low-Field Transport," *Solid-State Electronics*, vol. 41, no. 8, pp. 1139–1152, 1997.

[54] Y. Xuan *et al*., "Submicrometer Inversion-Type Enhancement-Mode InGaAs MOSFET With Atomic-Layer-Deposited Al_2O_3 as Gate Dielectric," *IEEE Electron Device Letters*, vol. 28, no. 11, pp. 935–938, 2007.

[55] S. Suthram *et al*., "Strain Additivity in III-V Channels for CMOSFETs beyond 22nm Technology Node," in *Symposium on VLSI Technology*, Honolulu, HI, USA, pp. 182–183, June 2008.

[56] L. Xia and J. A. del Alamo, "Mobility Enhancement in Indium-rich N-channel $In_xGa_{1-x}As$ HEMTs by Application of <110> Uniaxial Strain," in *International Conference on Indium Phosphide and Related Materials (IPRM)*, Takamatsu, Japan, pp. 1–4, May 2010.

[57] S. H. Kim *et al*., "Enhancement Technologies and Physical Understanding of Electron Mobility in III-V *n*-MOSFETs with Strain and MOS Interface Buffer Engineering," in *IEDM Technical Digest*, Washington, DC, USA, pp. 311–314, December 2011.

[58] C. Rossel *et al*., "Strain effects on *n*-InGaAs heterostructure-on-insulator made by direct wafer bonding," *Solid-State Electronics*, vol. 98, pp. 88–92, August 2014.

[59] A. Nainani *et al*., "Study of piezoresistance under uniaxial stress for technologically relevant III-V semiconductors using wafer bending experiments," *Applied Physics Letters*, vol. 96, no. 24, p. 242110, 2010.

[60] F. Schaffler, *Properties of Advanced Semiconductor Materials GaN, AlN, InN, BN, SiC, SiGe*, New York: John Wiley & Sons, 2001.

[61] M. Wagner, *Simulation of Thermoelectric Devices*, Ph.D. thesis, TU Vienna, Austria, November 2007.

[62] R. Cheaito *et al*., "Experimental Investigation of Size Effects on the Thermal Conductivity of Silicon-Germanium Alloy Thin Films," *Physical Review Letters*, vol. 109, no. 19, p. 195901, 2012.

[63] I. Yonenaga *et al*., "Thermal and Electrical Properties of Czochralski Grown GeSi Alloys," in *Proceedings of the 17th International Conference on Thermoelectrics (ICT)*, Nagoya, Japan, pp. 402–405, May 1998.

[64] P. D. Maycock, "Thermal Conductivity of Silicon, Germanium, III–V Compounds and III–V Alloys," *Solid-State Electronics*, vol. 10, no. 3, pp. 161–168, 1967.

[65] S.-M. Lee, D. G. Cahill, and R. Venkatasubramanian, "Thermal conductivity of Si–Ge superlattices," *Applied Physics Letters*, vol. 70, no. 22, pp. 2957–2959, 1997.

[66] C. Penn, T. Fromherz, and G. Bauer, *Properties of Silicon Germanium and SiGe:Carbon*, EMIS Datareviews Series, no. 12, London: INSPEC, 2000.

[67] O. A. Golikova, B. Ya. Moizhes, and L. S. Stil'bans, "Hole Mobility of Germanium as a Function of Concentration and Temperature," *Soviet Physics - Solid State*, vol. 3, no. 10, pp, 2259–2265, 1962.

[68] V. I. Fistul', M. I. Iglitsyn, and É. M. Omel'yanovskii, "Mobility of Electrons in Germanium Strongly Doped With Arsenic," *Soviet Physics - Solid State*, vol. 4, no. 4, pp. 784–785, 1962.

[69] S. M. Sze and J. C. Irvin, "Resistivity, Mobility and Impurity Levels in GaAs, Ge, and Si at 300° K," *Solid-State Electronics*, vol. 11, no. 6, pp. 599–602, 1968.

[70] L. Hutin *et al*., "Activation level in boron-doped thin germanium-on-insulator (GeOI): Extraction method and impact of mobility," *Materials Science in Semiconductor Processing*, vol. 11, no. 5–6, pp. 267–270, 2008.

[71] S. Mirabella *et al*., "Activation and carrier mobility in high fluence B implanted germanium," *Applied Physics Letters*, vol. 92, p. 251909, June 2008.

APPENDIX A Description of MCmob and SBmob PMI Models

This appendix describes the PMI models MCmob and SBmob, and their parameters.

Overview

The physical model interface (PMI) models `MCmob` and `SBmob` of Sentaurus Device are based on nonlinear relations between the mobility enhancement and the stress components where the coefficients of the equations are extracted from reference tools such as Sentaurus Band Structure (`SBmob`) or Sentaurus Device Monte Carlo (`MCmob`). The corresponding command file sections are explained in Chapter 3 on page 5.

The features of the PMI model `MCmob` are:

- Calculation of the hole mobility enhancement by stress for silicon and SiGe for mole fractions from 0% to 100% for the channel direction and wafer orientation combinations <110>/(001), <110>/(1$\underline{1}$0), and <100>/(001).
- Calculation of the electron mobility enhancement by stress for silicon for the channel direction and wafer orientation combinations <110>/(001), <110>/(1$\underline{1}$0), and <100>/(001).
- Crystallographic surface or interface orientation is determined automatically.

The features of the PMI model `SBmob` are:

- Calculation of the electron and hole mobility enhancement by stress for silicon and SiGe for mole fractions from 0% to 100% for the channel direction and wafer orientation combinations <110>/(001), <110>/(1$\underline{1}$0), and <100>/(001).
- Crystallographic surface or interface orientation is determined automatically.

The PMI models are designed for semiconductor–isolator interfaces as in an MIS structure where the bulk symmetry typical for the standard piezo model is broken. This makes it necessary to determine the direction of the interface normal with respect to the device coordinate system. Currently, this detection is not performed fully and automatically, and the specification of parameters in the Sentaurus Device parameter file is necessary (see Parameters on page 86).

Parameters

The PMI models allow the following parameter settings (same parameters and parameter syntax for `MCmob` and `SBmob`):

`autoorientation`	Switches detection of crystallographic surface orientation: `0`: No detection of crystallographic surface orientation, but crystallographic surface orientation is defined by `waferori` (default). `1`: Detection of crystallographic surface orientation. `2`: Detection of crystallographic surface orientation and adaptation of local coordinate system (coordinate system used to match the stress components to the MIS plane orientation and channel direction at each mesh node) for FinFET-like structures with <110> channel orientation. `3`: Detection of crystallographic surface orientation; local coordinate systems are defined using parameters in the Sentaurus Device parameter file.
`channelori`	Sets the channel direction: `110`: <110> (default) `100`: <100>
`waferori`	Sets the wafer orientation: `100`: (001) (default) `110`: (1$\underline{1}$0)
`coordinatesystem`	Global coordinate system in Sentaurus Device (default: `0`).
`ConstantMoleFraction`	Switches between reading the mole-fraction distribution from a TDR file and setting the constant mole fraction in the parameter file: `0`: Read from TDR file. `1`: User sets mole fraction in Sentaurus Device parameter file.
`ConstantStress`	Switches between reading the distribution of stress components from a TDR file and setting the constant stress components in the parameter file: `0`: Read from TDR file. `1`: User sets constant stress components in Sentaurus Device parameter file.
`DeltaMuPrefactorx`	Scales the mobility enhancement caused by stress in the current flow direction.

`DeltaMuPrefactory`	Scales the mobility enhancement caused by stress normal to the MIS interface.
`DeltaMuPrefactorz`	Scales the mobility enhancement caused by stress in-plane with the MIS interface and normal to the current flow direction.
`referenceplanecoordinatex1`	Coordinate of first reference plane in the x-direction of the device coordinate system (yz plane, default: 1e6).
`referenceplanecoordinatex2`	Coordinate of second reference plane in the x-direction of the device coordinate system (yz plane, default: 1e6).
`referenceplanecoordinatey1`	Coordinate of first reference plane in the y-direction of the device coordinate system (xz plane, default: 1e6).
`referenceplanecoordinatey2`	Coordinate of second reference plane in the y-direction of the device coordinate system (xz plane, default: 1e6).
`referenceplanecoordinatez1`	Coordinate of first reference plane in the z-direction of the device coordinate system (xy plane, default: 1e6).
`referenceplanecoordinatez2`	Coordinate of second reference plane in the z-direction of the device coordinate system (xy plane, default: 1e6).
`referenceplanesystemx1`	Defines the local coordinate system for the reference plane parallel to the yz plane at the position `x=referenceplanecoordinatex1` (default: –1).
`referenceplanesystemx2`	Defines the local coordinate system for the reference plane parallel to the yz plane at the position `x=referenceplanecoordinatex2` (default: –1).
`referenceplanesystemy1`	Defines the local coordinate system for the reference plane parallel to the xz plane at the position `y=referenceplanecoordinatey1` (default: –1).
`referenceplanesystemy2`	Defines the local coordinate system for the reference plane parallel to the xz plane at the position `y=referenceplanecoordinatey2` (default: –1).
`referenceplanesystemz1`	Defines the local coordinate system for the reference plane parallel to the xy plane at the position `y=referenceplanecoordinatez1` (default: –1).
`referenceplanesystemz2`	Defines the local coordinate system for the reference plane parallel to the xy plane at the position `y=referenceplanecoordinatez2` (default: –1).

`Stress_xx`	S_{xx} stress component in the device coordinate system when `ConstantStress=1`.
`Stress_yy`	S_{yy} stress component in the device coordinate system when `ConstantStress=1`.
`Stress_zz`	S_{zz} stress component in the device coordinate system when `ConstantStress=1`.
`MoleFraction`	SiGe mole fraction when `ConstantMoleFraction=1`.
`corrections`	Controls different ways of interpolation in the stress space. `corrections=0` (default) results in a linear superposition of the mobility response to the uniaxial stress components. `corrections=1` switches on cross-corrections (terms with mixed stress components). You must define the cross-corrections in the parameter file (default: all cross-corrections are set to zero). Currently, corrections are available for `MCmob` only.

For planar devices with one conducting MIS plane, the default parameters can be kept and no additional information is necessary when a device coordinate system has the configuration: x – channel direction, y – normal to the MIS interface, z – in-plane with the MIS interface but normal to the channel direction and the wafer orientation equals (100).

For other device coordinate systems and one conducting MIS plane, the parameter `coordinatesystem` must be specified in the Sentaurus Device parameter file:

- Device coordinate system:
  x: Channel direction
  z: Direction normal to the MIS interface
  y: In-plane with the MIS interface but normal to the channel direction (`coordinatesystem=1`)
- Device coordinate system:
  y: Channel direction
  x: Direction normal to the MIS interface
  z: In-plane with the MIS interface but normal to the channel direction (`coordinatesystem=2`)
- Device coordinate system:
  y: Channel direction
  z: Direction normal to the MIS interface
  x: In-plane with the MIS interface but normal to the channel direction (`coordinatesystem=3`)

- Device coordinate system:
  z: Channel direction
  x: Direction normal to the MIS interface
  y: In-plane with the MIS interface but normal to the channel direction (`coordinatesystem=4`)
- Device coordinate system:
  z: Channel direction
  y: Direction normal to the MIS interface
  x: In-plane with the MIS interface but normal to the channel direction (`coordinatesystem=5`)

For nonplanar devices with more than one conducting MIS plane, for example FinFETs, `autoorientation=2` provides automatic detection of the surface orientation and the coordinate system for FinFETs with <110> channel direction. For general applications and for FinFETs with channel direction <100> and wafer orientation (100), the local coordinate system must be defined manually in the Sentaurus Device parameter file by using the reference plane system parameters:

- Local coordinate system for a MIS interface in the xz plane close to `referenceplanecoordinatey1` or `referenceplanecoordinatey2`:
  x: Channel direction
  y: Direction normal to the MIS interface
  z: In-plane with the MIS interface but normal to the channel direction (`referenceplanesystemy1=0` or `referenceplanesystemy2=0`)
- Local coordinate system for a MIS interface in the xz plane close to `referenceplanecoordinatey1` or `referenceplanecoordinatey2`:
  z: Channel direction
  y: Direction normal to the MIS interface
  x: In-plane with the MIS interface but normal to the channel direction (`referenceplanesystemy1=1` or `referenceplanesystemy2=1`)
- Local coordinate system for a MIS interface in the xy plane close to `referenceplanecoordinatez1` or `referenceplanecoordinatez2`:
  x: Channel direction
  z: Direction normal to the MIS interface
  y: In-plane with the MIS interface but normal to the channel direction (`referenceplanesystemz1=0` or `referenceplanesystemz2=0`)
- Local coordinate system for a MIS interface in the xy plane close to `referenceplanecoordinatez1` or `referenceplanecoordinatez2`:
  y: Channel direction
  z: Direction normal to the MIS interface
  x: In-plane with the MIS interface but normal to the channel direction (`referenceplanesystemz1=1` or `referenceplanesystemz2=1`)

- Local coordinate system for a MIS interface in the yz plane close to `referenceplanecoordinatex1` or `referenceplanecoordinatex2`:
  y: Channel direction
  x: Direction normal to the MIS interface
  z: In-plane with the MIS interface but normal to the channel direction (`referenceplanesystemx1=0` or `referenceplanesystemx2=0`)
- Local coordinate system for a MIS interface in the yz plane close to `referenceplanecoordinatex1` or `referenceplanecoordinatex2`:
  z: Channel direction
  x: Direction normal to the MIS interface
  y: In-plane with the MIS interface but normal to the channel direction (`referenceplanesystemx1=1` or `referenceplanesystemx2=1`)

For the simulation of a planar MIS transistor, the use of the parameters `waferori` and `coordinatesystem` is sufficient. Instead of using `waferori`, `autoorientation=1` can be used to detect automatically the crystallographic wafer or surface orientation. In this case, `waferori` is overwritten by the automatically detected orientation. For FinFET devices with <110> channel direction, `autoorientation=2` can be used to allow automatic detection of the surface orientation and the local coordinate system. For other applications or for FinFETs with channel orientation <100>, the reference plan parameters can be used to define the local coordinate system where the crystallographic surface orientation is detected automatically. For that, `autoorientation=3` must be used.

The following examples illustrate the use of the parameters for orientation and coordinate system.

Example 1

Planar MISFET with wafer orientation (100) and device coordinate system x-channel direction, y-wafer normal direction, z-device width direction:

Default parameters can be used.

Example 2

Planar MISFET with wafer orientation (100) and device coordinate system x-channel direction, z-wafer normal direction, y-device width direction:

```
coordinatesystem=1
```

Example 3

Planar MISFET with wafer orientation (110) and device coordinate system with x-channel direction, z-wafer normal direction, y-device width direction:

```
coordinatesystem=1
autoorientation=1
```

or:

```
coordinatesystem=1
waferori=1
```

Example 4

FinFET with wafer orientation (100), channel orientation <110>, and device coordinate system with x-channel direction, y-wafer normal direction, z-fin width direction:

```
autoorientation=2
```

Example 5

FinFET with wafer orientation (100), channel orientation <110>, and device coordinate system with x-channel direction, z-wafer normal direction, y-fin width direction:

```
coordinatesystem=1
autoorientation=2
```

Example 6

FinFET with wafer orientation (100), channel orientation <100>, and device coordinate system with x-channel direction, z-wafer normal direction, y-fin width direction:

```
coordinatesystem=1
autoorientation=3
referenceplanesystemy1=0
referenceplanesystemy2=0
referenceplanesystemz1=0
referenceplanecoordinatey1=-@W/2.0@
referenceplanecoordinatey2=@W/2.0@
referenceplanecoordinatez1=@H@
```

Figure 50 shows a FinFET device with geometry.

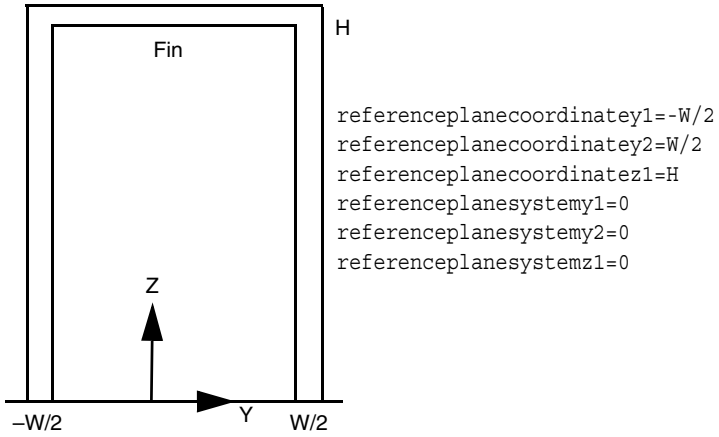

Figure 50 Cross section of FinFET structure normal to the channel direction with height (H) and width (W); the origin of the coordinate system is at y=0 and z=0

The PMIs have a parameter interface that allows you to change all coefficients of the fit and interpolation functions. In this way, you can define the mobility response to mechanical stress using the Sentaurus Device parameter file. For historical reasons, the syntax of the interface is different for `MCmob` and `SBmob`. The next section explains the parameter interface of `SBmob` and its related implementations and equations.

There are some settings that must be specified in the Sentaurus Device command file. First, the `Type` parameter is used to define the device type: NMOS (`Type=0`) or PMOS (`Type=1`). Second, the command `Kanda` switches on the Kanda model (refer to the *Sentaurus™ Device User Guide*).

Additional parameter files and explanations are available upon request. Contact TCAD Support (see Contacting Your Local TCAD Support Team Directly on page ix) or Consulting and Engineering (tcad-services@synopsys.com).

Parameter Interface and Equations of SBmob

The mobility response to the uniaxial stress components s_{xx}, s_{yy}, and s_{zz} is described by the following polynomial:

$$\frac{\Delta\mu}{\mu} = a_6 \cdot s_i^1 + a_5 \cdot s_i^2 + a_4 \cdot s_i^3 + a_3 \cdot s_i^4 + a_2 \cdot s_i^5 + a_1 \cdot s_i^6 \quad (4)$$

where i stands for xx, yy, or zz. Eq. 4 considers one stress component only and sets the other two stress components to zero.

The parameter interface allows for the definition of the coefficients of the polynomials for the mobility response to uniaxial stress. These coefficients have the names and meanings shown in Table 15. Note that not all the coefficients are shown in Table 15. However, the remaining coefficients that are not listed can be derived from the information in Table 15.

Table 15 Coefficients of polynomials for mobility response to uniaxial stress

Coefficient	Description
`aunics100c1106h`	Coefficient a_6 of the hole mobility response to stress in the channel direction for surface orientation (100) and channel direction <110>. The other five coefficients are named as follows: • `aunics100c1105h` • `aunics100c1104h` • `aunics100c1103h` • `aunics100c1102h` • `aunics100c1101h`
`aunins100c1101h`	Coefficient a_1 of the hole mobility response to the stress normal to the MIS interface for surface orientation (100) and channel direction <110>.
`auniws100c1101h`	Coefficient a_1 of the hole mobility response to stress in the width direction of the device for surface orientation (100) and channel direction <110>.
`auniws110c1101h`	Coefficient a_1 of the hole mobility response to stress in the width direction of the device for surface orientation (110) and channel direction <110>.
`auniws100c1001h`	Coefficient a_1 of the hole mobility response to stress in the width direction of the device for surface orientation (100) and channel direction <100>.
`auniws110c1001h`	Coefficient a_1 of the hole mobility response to stress in the width direction of the device for surface orientation (110) and channel direction <100>.

All a_i coefficients are mole fraction dependent. The mole fraction dependency can be defined in the parameter file using the following syntax (default: 11 mole fraction positions at 0, 0.1, 0.2, 0.3, 0.4, 0.5, 0.6, 0.7, 0.8, 0.9, 1.0):

a_i = (0, 1, 2, 3, 4, 5, 6, 7, 8, 9, 10) (arbitrary values are used here)

To improve the interpolation for high stress and for cases where the mobility response becomes independent of the stress or behaves linearly, additional parameters for the mobility response to uniaxial stress are introduced. In the parameter file, these coefficients have the same name and syntax as the parameters for the a_i coefficients but higher numbers. Their names and meanings are explained in Table 16 on page 94.

Table 16 Additional coefficients of polynomials for mobility response to uniaxial stress

Coefficient	Description
auniws100c1107h	Sets the negative stress value in GPa for the switch between the 6th order polynomial and linear slope for the hole mobility response to stress in the width direction of the device for surface orientation (100) and channel direction <110> (see Figure 51).
auniws100c1108h	Sets the slope in 1/Pa for the linear slope for stress values < auniws100c1107h for the hole mobility response to stress in the width direction of the device for surface orientation (100) and channel direction <110> (see Figure 51).
auniws100c1109h	Sets the positive stress value in GPa for the switch between the 6th order polynomial and linear slope for the hole mobility response to stress in the width direction of the device for surface orientation (100) and channel direction <110> (see Figure 51).
auniws100c11010h	Sets the slope in 1/Pa for the linear slope for stress values > auniws100c1109h for the hole mobility response to stress in the width direction of the device for surface orientation (100) and channel direction <110> (see Figure 51).

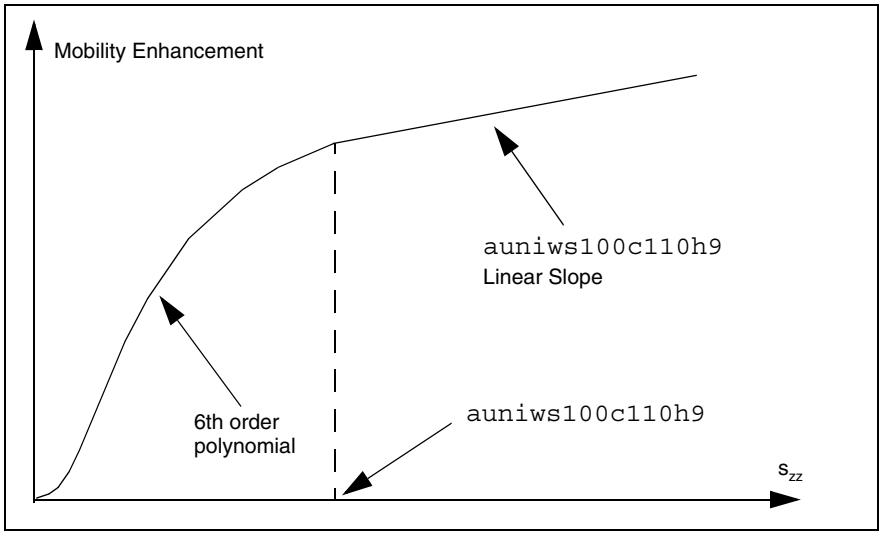

Figure 51 Use of the a_i parameters in fitting uniaxial stress curves